



HAL
open science

Study of transfer of alcohol (methanol, ethanol, isopropanol) during nanofiltration in water/alcohol mixtures

T.V.N. Nguyen, L. Paugam, P. Rabiller, M. Rabiller-Baudry

► **To cite this version:**

T.V.N. Nguyen, L. Paugam, P. Rabiller, M. Rabiller-Baudry. Study of transfer of alcohol (methanol, ethanol, isopropanol) during nanofiltration in water/alcohol mixtures. *Journal of Membrane Science*, 2020, 601, pp.117907. 10.1016/j.memsci.2020.117907 . hal-02499967

HAL Id: hal-02499967

<https://univ-rennes.hal.science/hal-02499967>

Submitted on 17 Mar 2020

HAL is a multi-disciplinary open access archive for the deposit and dissemination of scientific research documents, whether they are published or not. The documents may come from teaching and research institutions in France or abroad, or from public or private research centers.

L'archive ouverte pluridisciplinaire **HAL**, est destinée au dépôt et à la diffusion de documents scientifiques de niveau recherche, publiés ou non, émanant des établissements d'enseignement et de recherche français ou étrangers, des laboratoires publics ou privés.

Initially submitted to J. Membrane Science, August 7, 2019 (JMS-2019-2329)

Revised version R1- submitted November 2019

Revised version R2- submitted January 27, 2020

STUDY OF TRANSFER OF ALCOHOL (methanol, ethanol, isopropanol) DURING NANOFILTRATION IN WATER/ALCOHOL MIXTURES

Thi Vi Na NGUYEN¹, Lydie PAUGAM¹, Philippe RABILLER², Murielle RABILLER-BAUDRY^{1*}

1- Univ Rennes, CNRS, ISCR (Institut des Sciences Chimiques de Rennes) - UMR 6226,
F- 35000 Rennes, France

2- Univ Rennes, CNRS, IPR (Institut de Physique de Rennes) - UMR 6251, F-35000 Rennes,
France.

*Corresponding author : murielle.rabiller-baudry@univ-rennes1.fr

Table of Content

I.	Introduction.....	3
II.	Theoretical section	5
II.1.	Calculations for modelling of the alcohol rejections.....	5
II.1.1.	Film model to describe the transport of alcohol in the polarization layer	5
II.1.2.	Transfer of alcohol inside the membrane	7
II.2.	Analysis of flux decrease origins	10
III.	Experimental	14
III.1.	Membrane and NF pilot.....	15
III.2.	Water/alcohol filtered solutions (BGSs).....	15
III.3.	Analyses and alcohol rejection calculations	17
IV.	Results.....	17
IV.1.	Flux.....	17
IV.1.1.	Preliminary experiments	17
IV.1.2.	Experiments in standard conditions	18
IV.2.	Rejections	19

V.	Discussion	21
V.1.	Rejection and transfer modelling	21
V.1.1.	Rejections	21
V.1.2.	Mass transfert coefficients	21
V.1.3.	Membrane pore size estimation	26
V.2.	Flux decrease origin	28
V.2.1.	Osmotic pressure difference and membrane resistance determination	29
V.2.2.	Membrane swelling along different directions	30
VI.	Conclusion	33
	Acknowledgements	33
	Lists of symbols	34
	References	36
	Figures captions	41
	Table captions	42
	Supplementary informations	Error! Bookmark not defined.
	Supplementary 1 : viscosity of water/alcohol mixtures at 20°C	Error! Bookmark not defined.
	Supplementary 2 : dielectric constant of water/ethanol at 20°C	Error! Bookmark not defined.
	Supplementary 3 : Experimental flux (J_p) of water/alcohol mixtures	Error! Bookmark not defined.
	Supplementary 4 : mass transfer coefficient from correlations relating the Sherwood, Reynolds and Schmid numbers	Error! Bookmark not defined.
	Supplementary 5 : concentration polarisation by SD-F model	Error! Bookmark not defined.
	Supplementary 6 : pore radius value depending on the alcohol radii selected for the calculation	Error! Bookmark not defined.
	Supplementary 7: osmotic pressure detailed calculations for water/ethanol mixtures	Error! Bookmark not defined.
	Supplementary 8: osmotic pressure detailed calculations for water/methanol mixtures	Error! Bookmark not defined.
	Supplementary 9: osmotic pressure detailed calculations for water/isopropanol mixtures	Error! Bookmark not defined.

Highlights

- NF270 exhibits a selectivity between water and alcohol increasing with alcohol size
- Alcohols' rejections cannot be modelled by coupling Solution Diffusion and film models
- Alcohols' rejections are nicely modelled by coupling Spiegler & Kedem and film equations
- Viscosity & osmotic pressure have an impact on flux contrary to concentration polarisation
- Pore size & membrane thickness increase can compensate leading to a constant resistance

Abstract

This study aimed at studying the impact of alcohol presence in water/alcohol mixtures on the performances of the NF 270 polypiperazine amide nanofiltration membrane (Dow Filmtec). Three alcohols of different physico-chemical characteristics were selected: methanol, ethanol and isopropanol. NF was achieved for several water/alcohol mixtures of different viscosity (up to twice that of water) and dielectric constant, both known to play a role in separation performances. In presence of alcohol (up to 23 vol%, 30 vol% and 21 vol% for methanol, ethanol and isopropanol, respectively) the flux significantly decreased when compared to that of water. This study provides insights in the alcohol transfer mechanisms allowing to select Spiegler & Kedem and reject Solution-Diffusion, both coupled with the film theory. Discussion highlights how surprisingly the membrane swelling can sometimes have no significant impact on the membrane resistance because opposite phenomena can be compensated such as pore radius increase simultaneously with membrane thickness increase.

Keywords: nanofiltration; water/alcohol mixtures; flux; transfer mechanisms; modelling

1. Introduction

Nowadays, in biotechnology, cosmetology and pharmacy, the demand increases to develop the extraction of bio-molecules, from renewable resources such as plants, seaweed and co-products of agro-food industries, aiming at fulfilling the green chemistry recommendations [1, 2]. Because, water as extraction solvent is often not efficient enough, the use of organic solvents, either pure or in mixture, is generally required. Bio-industry is more and more interested in using ethanol that can be itself bio-sourced and thus allows having more sustainable processes together with a better quality of the final product. To obtain high added-value extracts from raw materials, additional purification and concentration are generally required. Performed at room temperature

limiting energy consumption, Nanofiltration becomes an appropriate alternative to conventional separation processes such as chromatography, evaporation, crystallization and distillation [3, 4].

Nanofiltration (NF) has a lot of applications in environment, desalination, food industry, etc.[5]. In water media, NF mastering at large industrial scale is a reality and the level of fundamental understanding of separations is good. The irreversible thermodynamic approach is often used to model transfer of neutral solutes whereas the extended Nernst-Planck equation is used to describe that of charged solutes [6, 7]. Organic Solvent Nanofiltration (OSN) is an emerging process and has far less industrial applications. Today, OSN can be used in solvent recovery, solute enrichment, pharmaceutical purifications, etc. [5, 8-13]. Mastering at large industrial scale is more difficult than for aqueous applications because (1) of safety requirements, (2) of the rather low level of fundamental understanding of separations, and (3) of the lack of commercially available membranes. The sufficiently resistant dense membranes are generally made of hydrophobic polydimethylsiloxane (PDMS) or more hydrophilic polyimide but are often not enough selective for a wide application range. The solution diffusion model is often used to model transfer in OSN but clearly physico-chemical complex interactions in the membrane-solute-solvent system have to be taken into account.

To minimize the organic solvent consumption and simultaneously increase the extraction efficiency, the use of water/alcohol mixtures can be developed [3, 14]. Thus, NF in water/ethanol achieved in limited amount of ethanol could be interesting at industrial level specially when using commercial membranes of aqueous applications. Such hydro-organic NF, bridging aqueous NF and OSN could be called “Solvent Tolerant Nanofiltration” (STNF) as very recently proposed by Prof. Yvo Vankelecom [15]. STNF appeared as an emerging field for nanofiltration, for which only few fundamental knowledge is available. The transfer of neutral and charged solutes across NF membranes in water/ethanol mixtures is only sparsely documented and only few studies have reported on transfer in hydro-organic media. They concern (i) the transfer of hydro-organic binary mixtures through dense polymer membranes or porous ceramic ones [16-18], (ii) the permeation flux and rejection of various organic solutes in water/ethanol mixtures with organic membranes [19-21]. Despite these previous works, to date, the transport/transfer mechanisms are not comprehensively understood in water/alcohol mixtures. Together with the impact of ethanol presence on the overall viscosity of the filtered media, decreasing all transport velocities such as those by convection and diffusion, the modification of the solvent dielectric constant might have an impact on the electrostatic interactions and the dissociation of ion pairs. Moreover, solvation of solutes and membranes might be modified in presence of ethanol, when compared to pure water. Ethanol might induce solute size variation but also physical changes of the membrane because of the variation of the mobility of the polymer chains due to the influence of the organic solvent inducing for instance the membrane swelling. If this diagnostic is easy to do, the effective impact is not easy to accurately imagine and simulate and there is a major scientific gap to be fulfilled. Indeed, modulation of transport and transfer mechanisms due to ethanol presence could have an impact on both flux and selectivity. The polypiperazine amide

membrane, NF 270 provided by Dow Filmtec, is a well-known membrane in water applications. It was selected because it is known to have a high cross-linked degree expecting at the limitation of the membrane swelling aiming at depicting other effects. Nevertheless, even if the membrane is generally described as porous [22-23], can it evolve toward a dense membrane as a consequence of swelling? To be able to use classical filtration loop in safe conditions, the ethanol amount was voluntary limited to 30 vol% corresponding to 5.13 mol.L⁻¹. However, the increase of ethanol amount induced a significant increase of the viscosity that can be up to twice that of water (see **Supplementary 1**, [24-26]). Simultaneously the dielectric constant decreased from $\epsilon_r = 80$ in pure water to about 63 in 30 vol% ethanol (see **Supplementary 2**, [27]). In order to decouple the role of the viscosity and that of the dielectric constant, NF of water/alcohol binary systems of same viscosity was achieved using ethanol, methanol and isopropanol (see **Supplementary 1** and **Supplementary 2** for viscosities and dielectric constants). This paper aims at providing a fundamental study of the water/alcohol behaviour in STNF as a first step for understanding the impact of this background solvent (BGS) on the transfer of other solutes dissolved in the BGS, knowing that a significant separation between water and alcohol cannot be expected.

II. Theoretical section

II.1. Calculations for modelling of the alcohol rejections

Regardless of the membrane structure the rejection is partly controlled by the driving forces in the concentration polarization layer and those acting inside the membrane and inducing convection, diffusion etc. The transport in the concentration polarization (CP) layer was assumed to be based on convection + diffusion and was described with respect to the film theory that must further be coupled with another model applied to describe the transfer in the membrane. Depending on the membrane structure, either dense or porous, different models might be used to explain the alcohol rejection. We have voluntary chosen to *a priori* test two transfer models that are briefly given below. Their selection was motivated by the classical choices made to describe transfers in literature dealing with OSN:

(i) solution diffusion requiring a behaviour similar to that of a dense membrane, knowing that we don't want to assume any given structure for the NF270 membrane in water/alcohol mixtures even if it is generally described as a porous membrane in aqueous NF.

(ii) irreversible thermodynamic based on the Spiegler & Kedem model requiring no assumption on the membrane structure.

II.1.1. Film model to describe the transport of alcohol in the polarization layer

If any concentration polarisation occurs, the concentration of the solute at the membrane wall (C_m) will increase when compared to its concentration in the bulk (C_b). The relation between the two concentrations can be calculated by using the film theory:

$$\frac{C_m - C_p}{C_b - C_p} = \exp\left(\frac{J_p}{k}\right) \quad (\text{eq. 1})$$

With:

C_m : solute concentration at the membrane wall

J_p : permeate volumic flux

C_p : concentration in the permeate

C_b : concentration in the retentate

k : mass transfer coefficient in the concentration polarization layer

$$k = D/\delta_{CP} \quad (\text{eq. 2})$$

With:

D : diffusion coefficient of the neutral solute in the polarization layer

δ_{CP} : the thickness of the polarization layer

Consequently, after rearrangement of **eq.1** the following equation expressed the relation between the observed (or experimental) rejection (R_{obs}) and the real rejection (R_{real}):

$$\frac{1-R_{obs}}{R_{obs}} = \frac{1-R_{real}}{R_{real}} \exp\left(\frac{J_p}{k}\right) \quad (\text{eq. 3})$$

With:

$$R_{real} = 1 - \frac{C_p}{C_m} \quad (\text{eq. 4})$$

$$R_{obs} = 1 - \frac{C_p}{C_b} \quad (\text{eq. 5})$$

Then after rearrangement the observed rejection can be written according to:

$$R_{obs} = \frac{R_{real}}{(1 - R_{real}) \exp\left(\frac{J_p}{k}\right) + R_{real}} \quad (\text{eq. 6})$$

Thus C_m can be calculated according to:

$$C_m = C_b \frac{(1 - R_{obs})}{(1 - R_{real})} \quad (\text{eq. 7})$$

The thickness of the polarization layer (δ_{CP}) can be calculated using different approaches. For instance, by using dimensionless numbers [28, 29]. However, the approach privileged here consisted in the use of experimental data thanks to the R_{exp} vs J_p plot. k was obtained by fitting experimental data to calculated one using **eq. 6**. Then, the thickness of the polarization layer can be calculated by **eq. 2**.

When considering that the transfer inside the membrane was obtained by coupling solution-diffusion (SD) and film equations (see below) then δ_{SD-F} was calculated by **eq. 2** substituting k by k_{SD-F} . Quite similarly, δ_{SK-F} was given by coupling Spiegler & Kedem (SK) and film equations leading to k_{SK-F} .

II.1.2. Transfer of alcohol inside the membrane

II.1.2.1. Solution Diffusion (SD) model

This model was initially proposed to describe transfer through dense membranes of aqueous RO for which the driving force is the gradient in solute concentration across the membrane thickness [30]. The real rejection of a solute can be calculated by the following equation:

$$R_{real,SD} = \frac{J_p}{J_p + P_{SD}} \quad (\text{eq. 8})$$

With:

$R_{real,SD}$: real rejection (see **eq. 4** for definition) deduced from the SD model.

P_{SD} : solute transfer coefficient in the membrane obtained via the SD model and often called solute permeability. The SD subscript refers to the solution-diffusion model.

In presence of concentration polarisation, the combination of equations of SD and film models was achieved as proposed by [31]. By replacing R_{real} in the film equation by its expression in SD (**eq. 8**) then **eq. 3** evolved in the following one, in which the subscript SD-F refers to the combination of solution-diffusion and film models:

$$\frac{1 - R_{obs}}{R_{obs}} = \frac{P_{SD-F}}{J_p} \exp\left(\frac{J_p}{k_{SD-F}}\right) \quad (\text{eq. 9})$$

Thanks to the "Solver" function of Excel, the two parameters k_{SD-F} and P_{SD-F} were adjusted to fit the experimental rejections (R_{exp}) from their plot versus J_p obtained from the experimental data at different pressures (**Table 1**). Then, the real rejection deduced from this combination ($R_{real,SD-F}$) was calculated by **eq. 8** in which $R_{real,SD}$ and P_{SD} were substituted by $R_{real,SD-F}$ and P_{SD-F} .

Table 1: Parameters required for calculations and deduced by the different models: Solution Diffusion + Film (SD-F), Spiegler & Kedem + Film (SK-F), Steric Hindrance pore (SHP)

Models	Entry		Fitting parameters (Excel solver)	Other obtained parameters
	literature data	experimental data		
SD-F	-	R_{exp}, J_p	k_{SD-F}, P_{SD-F}	$R_{real,SD-F}$ $R_{obs,SD-F}$
SK-F + SHP	r_s^*	R_{exp}, J_p	$k_{SK-F}, P_{SK-F}, \sigma_{SK-F}$	$R_{real,SK-F},$ $R_{obs,SK-F}$ $r_p, \frac{\Delta e}{A_k}$

*: r_s is the solute radius

II.1.2.2. Spiegler & Kedem (SK) model

The Spiegler & Kedem (SK) model based on the irreversible thermodynamic was developed in 1966 [32]. In this model, the membrane is considered as a black box and no parameter describing the membrane structure are required partly explaining why the SK equation has often been used in literature to describe the transfer of neutral solutes in aqueous solution particularly in NF. Local fluxes, either that of solvent or that of a single solute dissolved in the solvent can be independently expressed according to the following equations:

$$J_p = -L_{solvent} \left(\frac{dP}{dx} - \sigma \frac{d\pi}{dx} \right) \quad (\text{eq. 10})$$

And

$$J_{solute} = -P_{local} \frac{dC}{dx} + (1 - \sigma) C J_{solvent} \quad (\text{eq. 11})$$

With:

J_p : permeate volume flux. In the present study the water/alcohol mixture will be assimilated to a background solvent hereafter denoted BGS owing a viscosity equal to that of the water/alcohol mixture

J_{solute} : solute flux

$L_{solvent}$: membrane permeability to solvent

P: pressure

x: coordinate along the membrane thickness axis

σ : reflection coefficient of the solute by the membrane.

C: solute concentration

π : osmotic pressure due to the solute

P_{local} : the local permeability of the solute (dimension corresponding to that of a diffusion coefficient)

Assuming that P_{local} and σ are independent of the concentration and that $P_{SK} = \frac{P_{local}}{\Delta x}$, integration of **eq. 10** and **eq. 11** was achieved with the following limiting conditions: $C = C_m$ when $x = 0$ and $C = C_p$ (concentration in permeate) when $x = \Delta x$ (the membrane active layer thickness). Then the real rejection of the solute can be calculated by the following equation:

$$R_{real,SK} = 1 - \frac{(1-\sigma_{SK})}{1-\sigma_{SK} \exp[(\sigma_{SK}-1) \left(\frac{J_p}{P_{SK}}\right)]} = \frac{(1-F) \sigma_{SK}}{1-F \sigma_{SK}} \quad (\text{eq. 12})$$

With:

$$F = \exp\left[-(1-\sigma_{SK}) \frac{J_p}{P_{SK}}\right] \quad (\text{eq. 13})$$

σ_{SK} : the reflection coefficient of the solute by the membrane obtained from the SK model

P_{SK} : global solute permeability in the membrane according to the SK model. The subscript SK refers to the Spiegler- Kedem model

To give a physical meaning and interpret σ_{SK} and P_{SK} , several models were previously proposed.

The steric-hindrance pore (SHP) model providing a description for a porous membrane [33] was used in the present study. SHP model considers that during the transport, a neutral solute has certain steric hindrance and interactions with the pore wall. A solute with the same or larger size as the pore size would be completely rejected, whereas a solute smaller than the pore would be partially retained due to these effects. The reflection coefficient was then calculated by **eq. 14** allowing the determination of the membrane pore radius (knowing that of the solute).

$$\sigma_{SHP} = 1 - \left(1 + \frac{16r_s^2}{9r_p^2}\right) \left(1 - \frac{r_s}{r_p}\right)^2 \left[2 - \left(1 - \frac{r_s}{r_p}\right)^2\right] \quad (\text{eq. 14})$$

With:

σ_{SHP} : the reflection coefficient of the solute by the membrane obtained from the SHP model

r_p : average membrane pore radius

r_s : neutral solute radius, here that of alcohol.

In presence of concentration polarisation, the real rejection ($R_{real,SK-F}$) was calculated by combination of the equations of SK and film models. The fitting parameters (k_{SK-F} , P_{SK-F} , σ_{SK-F} , **Table 1**, in which the subscript SK-F refers to the combination of Spiegler&Kedem and film models) were adjusted to ensure that the calculated observed rejections (obtained by the film model equation in which the used real rejection was those obtained from the SK equation) fitted as close as possible to the experimental rejections. The final expression of $R_{real,SK-F}$ is given by **eq. 12** in which $R_{real,SK}$ and P_{SK} were substituted by $R_{real,SK-F}$ and P_{SK-F} , respectively.

II.2. Analysis of flux decrease origins

When measuring the membrane flux to pure water, the Darcy law is fulfilled and:

$$J_{p,water} = L_{p,water} \text{TMP} = \frac{\text{TMP}}{\eta_{water} R_{m,water}} \quad (\text{eq. 15})$$

With:

$J_{p,water}$: permeate flux in water ($\text{m}\cdot\text{s}^{-1}$)

$L_{p,water}$: the membrane permeance in water ($\text{m}\cdot\text{s}^{-1}\cdot\text{Pa}^{-1}$)

TMP: transmembrane pressure (Pa)

$R_{m,water}$: membrane hydraulic resistance in water (m^{-1})

η_{water} : water viscosity (Pa.s)

During filtration of water/alcohol mixtures also hereafter called background solvents (BGSs), with respect to both the viscosity variation and the alcohol rejection and in absence of irreversible fouling (general case in the following) **eq. 15** evolved in:

$$J_{p,BGS} = L_{p,BGS} (\text{TMP} - \Delta\pi) = \frac{(\text{TMP} - \Delta\pi)}{\eta_{p,BGS} R_{m,BGS}} \quad (\text{eq. 16})$$

With:

$J_{p,BGS}$: permeate flux in the given BGS (water/alcohol mixture) ($\text{m}\cdot\text{s}^{-1}$)

$L_{p,BGS}$: the membrane permeance in BGS ($\text{m}\cdot\text{s}^{-1}\cdot\text{Pa}^{-1}$)

TMP: transmembrane pressure (Pa)

$R_{m,BGS}$: membrane hydraulic resistance in the given BGS assuming possible variation due to swelling in presence of an organic solvent (m^{-1})

$\eta_{p,BGS}$: permeate viscosity when filtering the given BGS (Pa.s) calculated from experimental data given in **Supplementary 1** taken from [24-26].

$\Delta\pi$: the difference in osmotic pressure due to the alcohol rejection (Pa)

The van't Hoff equation commonly used to calculate the osmotic pressure is only reliable for solutions up to 1 mol.L⁻¹. For higher concentrations, it can be defined with a better accuracy by considering the activity coefficients [34] or the virial expansion reduced to the 1st virial coefficient [35, 36]. This last possibility was selected in the present work:

$$\frac{\pi_i}{R(\text{gas})T} = C_i + \frac{1}{2} B' C_i^2 \quad (\text{eq. 17})$$

With:

π_i : osmotic pressure due to solute i (Pa)

R(gas) : gas constant (8.314 J.K⁻¹. mol⁻¹)

T: temperature (K)

C_i : concentration of solute i (mol.m⁻³)

$\frac{1}{2} B'$: second virial coefficient (m³.mol⁻¹)

B' represents the exclusion volume of the solute [35, 36-39]. As a first assumption, B' can be chosen equal to the molar volume (V_m) calculated from the density (ρ , **Table 2**).

At low concentration **eq.17** evolved in the well-known limiting law called the van't Hoff equation as the first term of the virial expansion ($\frac{1}{2} B' C_i^2$) becomes negligible.

Table 2: Properties of pure solvents (Stokes radius in water ($r_{s,Stokes}$), viscosity η , density ρ , Hildebrand solubility parameter δ , molar volume V_m at 20°C.

	$r_{s,Stokes}$ (nm)	η (mPa.s)	ρ (g.cm ⁻³)	δ (J.cm ⁻³) ^{1/2}	V_m (10 ⁻⁵ .m ³ .mol ⁻¹)
Compound	[40]	[24-26]	[24-26, 41]	[17]	[42]
Water	0.17	1.005	1.000	47.8	1.80
Methanol	0.26	0.585	0.792	29.6	4.05
Ethanol	0.31	1.189	0.791	26.5	5.82
Isopropanol	0.40	2.414	0.785	23.5	7.65

However, V_m values correspond to pure alcohols and as solvation and hydrogen bonding, might evolved in water/alcohol, B' could probably also evolved. The question is now: how to evaluate B' in the solvent binary mixture? We assumed to calculate a third value hereafter noticed

limiting volume ($V_{m,BGS}$) corresponding to the volume of an equivalent molecule of the BGS by the mean of the following equation:

$$V_{m,BGS} = x_{water}V_{m,water} + x_{alcohol}V_{m,alcohol} \quad (\text{eq. 18})$$

With:

$$V_{m,water} = B' \text{ for pure water} = 1.80 \cdot 10^{-5} \text{ m}^3 \cdot \text{mol}^{-1}$$

$$V_{m,alcohol} = B' \text{ for pure alcohol} = V_m \text{ in } \text{m}^3 \cdot \text{mol}^{-1}.$$

x_{water} and $x_{alcohol}$ the molar fraction of water and alcohol in the BGS, respectively

Fig. 1 depicts the $V_{m,BGS}$ (and thus B') variation with respect to the alcohol nature and content in water. Regardless of the alcohol, below 30 vol% $V_{m,BGS}$ varies only a few and average values can be drawn for each alcohol (**Table 3**, **Table 4**).

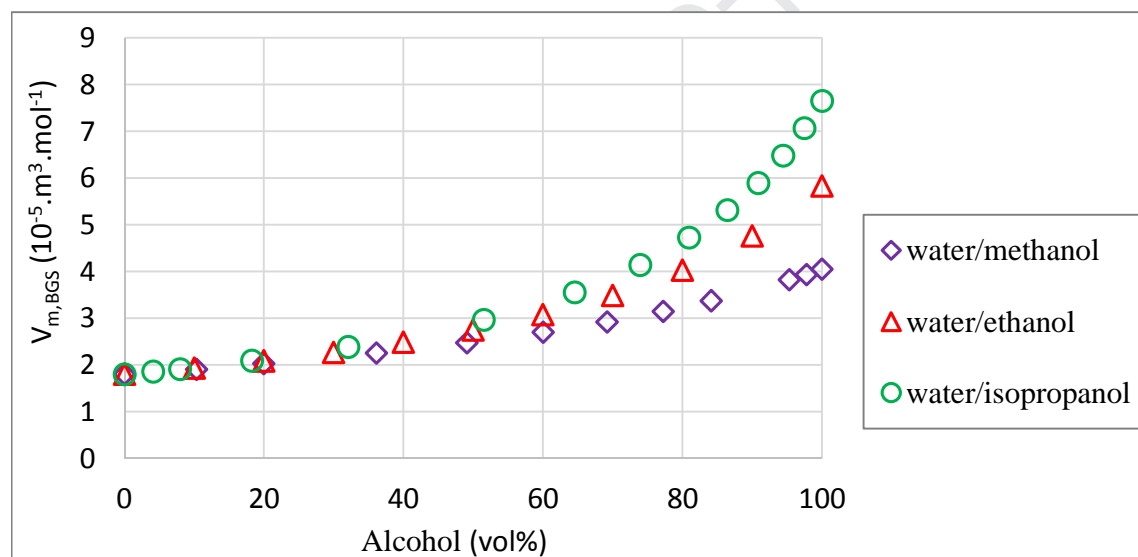


Fig. 1: Equivalent molar volumes of BGS calculated from density of pure solvents and from **eq. 18**.

Fig. 2 depicts the evolution of the osmotic pressure according to **eq. 17** in the concentration ranges corresponding to the alcohol molar concentration ranges of the present study.

Clearly, as it is well-known, the van't Hoff equation can be considered as a nice approximation up to $1 \text{ mol} \cdot \text{L}^{-1}$. In the concentration range of the present study, the maximum deviation between van't Hoff approximation and the virial expansion is obtained when using $B'=V_m$ for each

alcohol and is 6% for methanol (MeOH), 15% for ethanol (EtOH) and 11% for isopropanol (i-PrOH).

In the following all calculations of the osmotic pressure difference will be made by using 3 different values of B' (van't Hoff, $V_{m,BGS}$, V_m) for sake of comparison (**Table 4**). Of course, if any concentration polarization exists, it must be taken into account in the osmotic pressure on the retentate side and $\Delta\pi_{obs}$ determined from the bulk concentration in the feed has to be replaced by $\Delta\pi_{real}$ calculated from the concentration at the membrane wall in **eq. 16** for the further determination of the membrane resistance.

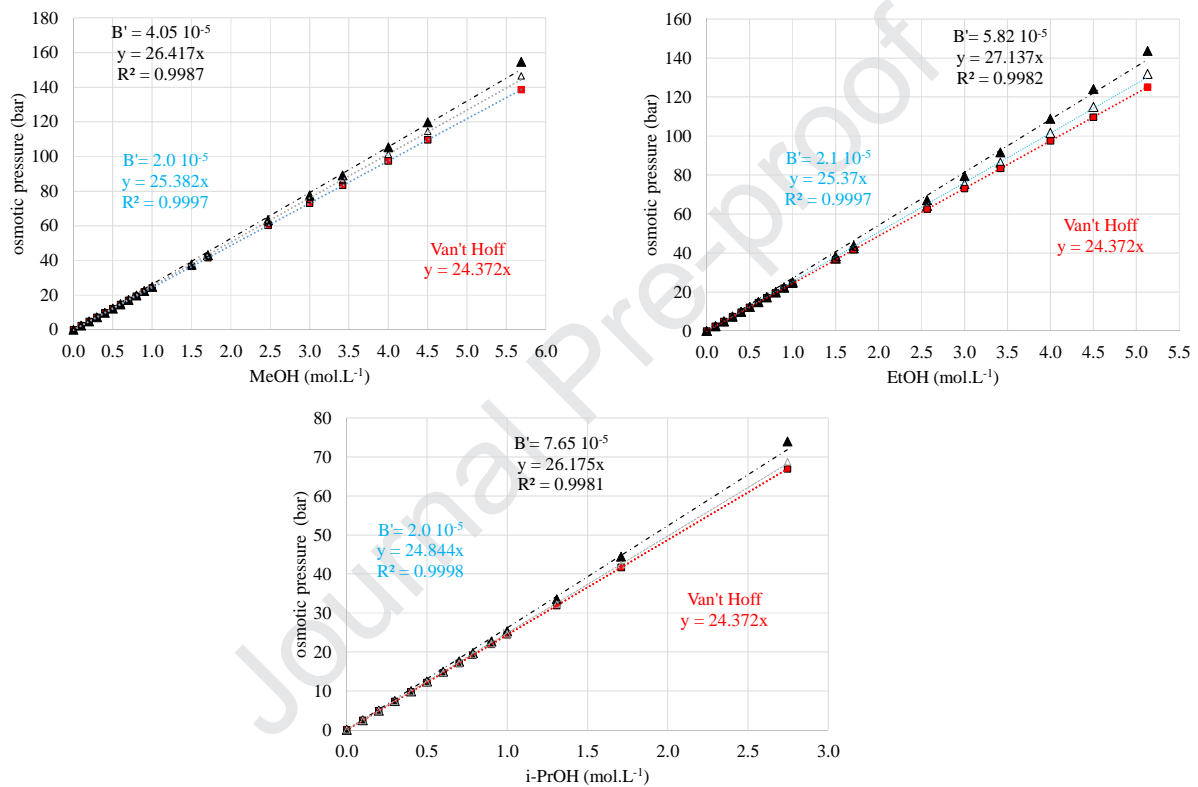


Fig. 2: Osmotic pressure at 20°C calculated according to van't Hoff equation (■) and taking into account virial expansion reduced at its first terms (**eq. 17**) in the range of the present study with $B' = V_m$ (▲) and $B' = V_{m,BGS}$ (△), (**Table 3**, **Table 4**).

Table 3 : Properties of water/alcohol mixtures (BGS) at 20°C: viscosity η_{BGS} , diffusion coefficient of alcohol in the polarization layer taking into account slight polarisation D_{alcohol} , density, ρ_{BGS} (eq. 20), Hansen-Hildebrand solubility parameter (eq. 21), δ_{BGS} and equivalent molar volume $V_{\text{m,BGS}}$ of the solvent mixture (eq. 18).

water/alcohol v/v	[alcohol] (mol.L ⁻¹)	η_{BGS} (mPa.s)	D_{alcohol} (10 ⁻¹⁰ .m ² .s ⁻¹)	ρ_{BGS} (g.cm ⁻³)	δ_{BGS} (J.cm ⁻³) ^{1/2}	$V_{\text{m,BGS}}$ (10 ⁻⁵ m ³ .mol ⁻¹)	
water/ methanol	90/10	2.55	1.289	6.53	0.979	45.98	1.91
	77/23	5.71	1.593	5.28	0.952	43.64	2.06
water/ ethanol	90/10	1.72	1.289	5.37	0.979	45.73	1.93
	85/15	2.57	1.593	4.34	0.968	44.66	2.01
	80/20	3.43	1.811	3.82	0.958	43.59	2.09
	70/30	5.13	2.313	2.99	0.937	41.46	2.27
water/ isopropanol	94/6	0.75	1.289	4.21	0.988	46.47	1.89
	90/10	1.35	1.593	3.41	0.978	45.35	1.95
	79/21	2.78	2.313	2.35	0.954	42.67	2.14

Table 4: selected B' values (10⁻⁵ m³.mol⁻¹) according to assumptions

	methanol	ethanol	isopropanol
B' pure alcohol (V _m)	4.05	5.82	7.65
B' average BGS (V _{m,BGS}) (alcohol range vol%)	2.0 ± 0.2 (10-23 vol%)	2.1 ± 0.2 (10-30 vol%)	2.0 ± 0.2 (6-21 vol%)

III. Experimental

Nanofiltration experiments were achieved in classical conditions commonly encountered for aqueous applications. To be able to perform NF in safe conditions on a pilot initially designed for aqueous filtration, the ethanol amount was voluntary limited to 30 vol%. Concentration of MeOH and i-PrOH were selected to have similar viscosity when compared to some of the EtOH based BGSs.

III.1. Membrane and NF pilot

The flat membrane used was a NF 270 (polypiperazine amide, MWCO 150-180 g.mol⁻¹ [22, 23], 140 cm² filtering area) from Dow FilmTec (USA).

The cross-flow filtration pilot was an assembly of a Millipore Proscale pilot and a plate and frame filtration cell (SEPA CF II, Osmonics, USA). A spacer of 1.2 mm thickness (47 mil type provided by the manufacturer of the SEPA cell, Osmonics) was inserted in the liquid channel on the retentate/feed side to create local turbulences. In standard conditions, the recirculation feed flow rate was set at 325 ± 5 L.h⁻¹ inducing an estimated cross-flow velocity in the free liquid channel of $v = 0.50 \pm 0.01$ m.s⁻¹. The temperature was set at 20 ± 1 °C and the transmembrane pressure (TMP) varied between 4 and 28 bar.

In standard conditions (and except specific comments) the flat membrane was stocked overnight in the appropriate water/alcohol mixture before starting the filtration. Moreover, the permeate flux was systematically recorded with time at each pressure until a plateau value was reach (that was quite instantaneous or at least needed less than 5 min). Flux measurements were measured with an accuracy of 2% by sampling permeate during a given time and weighting.

III.2. Water/alcohol filtered solutions (BGSs)

The properties of pure solvents are given in **Table 2**. NF was carried out in water, and water/alcohol binary mixtures prepared by mixing water previously demineralized and 1 µm filtered and the corresponding alcohol (**Table 5**).

Table 5: Quality of alcohols

Solvent	Provider	Molecular weight (g.mol ⁻¹)	Purity (vol%)
Methanol	Sigma-Aldrich	32.04	99.6
Ethanol	VWR	46.07	96.0
Isopropanol	Sigma-Aldrich	60.01	99.5

The properties of the water/alcohol mixtures are given in **Table 3**. They have been calculated from data of **Table 2** by considering an ideal mixing of the two solvents as it is classically done in literature.

The diffusion coefficient of alcohol (D) was calculated by the mean of the Stokes equation at infinite dilution (that is of course a strong assumption, see also discussion):

$$D = \frac{k_B T}{6\pi\eta r_{s,Stokes}} \quad (\text{eq. 19})$$

With:

$k_B = 1.38 \times 10^{-23} \text{ J.K}^{-1}$, Boltzmann constant

T: temperature (K)

η : viscosity of the solvent mixture (BGS) taken as the same as in the bulk. This assumption was justified *a posteriori* by the low intensity of the polarization phenomenon.

$r_{s,Stokes}$: Stokes radius of alcohol measured in water that is of course another strong assumption (**Table 2**)

The density ρ_{BGS} of a solvent mixture was calculated by considering an ideal mixing of the two solvents as it is commonly shown in literature when dealing of binary mixtures:

$$\rho_{BGS} = \frac{(\text{vol}\%_{\text{water}}\rho_{\text{water}} + \text{vol}\%_{\text{alcohol}}\rho_{\text{alcohol}})}{100} \quad (\text{eq. 20})$$

With:

ρ_i and $\text{vol}\%_i$: the density and volume percentage of solvent 'i', respectively

Values of density of pure solvent were taken from the literature (**Table 3**). It is noticeable that the density calculated from **eq. 20** for water/ethanol mixtures were very slightly overestimated when compared to the experimental density given in [43]; the maximum error was 2.5 % at 30 vol% ethanol. Consequently the molar volume ($V_{m,BGS}$) was slightly underestimated by using **eq. 18** but without any significant impact on the average value over the studied ethanol range. Similarly, the density of water/methanol mixtures calculated from **eq. 20** were quite close to the experimental data given in [44]; the maximum error was 1.6 % at 23 vol% methanol. Finally, the density of water/isopropanol mixtures calculated from **eq. 20** were compared to the experimental data given in [45]; **eq. 20** slightly underestimated the density, however the maximum error was 1.6 % at 21 vol% isopropanol. So as for ethanol, there was no significant impact on the average value ($V_{m,BGS}$) over the studied methanol and isopropanol ranges, respectively.

The Hansen-Hildebrand solubility parameters, δ_{BGS} , of the solvent mixtures were calculated by **eq. 21** as proposed by Vandezande *et al.* [46] and also used by Soroko *et al.* [47]. The obtained values (**Table 3**) were similar to those calculated by Romero [48].

$$\delta_{\text{BGS}} = \frac{x_{\text{water}}V_{\text{m,water}}\delta_{\text{water}} + x_{\text{alcohol}}V_{\text{m,alcohol}}\delta_{\text{alcohol}}}{x_{\text{water}}V_{\text{m,water}} + x_{\text{alcohol}}V_{\text{m,alcohol}}} \quad (\text{eq. 21})$$

With:

x_i and $V_{\text{m},i}$ the molar fraction and the molar volume of solvent 'i', respectively.

Values of molar volume of pure solvent were calculated from the density and were similar to those taken from the literature (**Table 2**) [42, 49].

III.3. Analyses and alcohol rejection calculations

Alcohols were quantified by HPLC with an accuracy better than 5% using a column made of a sulfonated polystyrene ligand exchanger gel bearing Ca^{2+} counter-ions (SUGAR SC1011, 8.0 mm x 300 mm i.d. x L, Shodex). The isocratic elution was achieved by ultra-pure water at 65°C at 1.3 mL.min⁻¹. 20 µL sample volumes of 0.45 µm filtered retentate or permeate were injected (in this condition, there is no evaporation of alcohol during the analysis). Detection was achieved by a RI detector. These analyses allowed to determine the experimental alcohol rejection (R_{exp}) using **eq. 5** and substituting R_{obs} by R_{exp} , with an accuracy better than 10%

IV. Results

NF of all BGS was achieved in standard conditions. Nevertheless, results and discussion are mainly focused on water/alcohol mixtures of selected viscosities: $\eta = 1.289$ mPa.s, 1.593 mPa.s and 2.313 mPa.s that are common values for some selected BGSs based on different alcohols.

IV.1. Flux

IV.1.1. Preliminary experiments

Several filtrations were achieved in which the cross-flow velocity (as estimated in free channel) was varied from 0.16 m.s⁻¹ to 0.57 m.s⁻¹ including 0.50 m.s⁻¹ further used as standard condition. For water/methanol 77/23, water/ethanol 70/30 and water/isopropanol 90/10 exhibiting quite high viscosity (**Table 3**), flux measurements (not detailed here) evidenced no impact of the presence or absence of the retentate spacer inserted in the liquid channel. These results suggested a low polarization over the studied velocity and viscosity ranges.

Moreover, several consecutive cycles of NF were achieved either with pure water or with water/alcohol. When filtering water/alcohol the experimental flux systematically and decreased in less than 5 min when compared to that measured in pure water. After a very short water rinsing, the permeate flux to water was fully recovered.

We have previously studied the impact of ethanol on a PES/PVP ultrafiltration membrane. When achieving cycle of consecutive water flux, water/ethanol 70/30 flux then once again water flux, it

was clearly evidenced that the UF membrane cannot recovered instantaneously its initial resistance in water after immersion in water/ethanol. The de-swelling was not instantaneous for such not cross-linked UF membrane and required several hours (not shown).

Finally, these results suggested a low impact of alcohol on the NF 270 membrane swelling and the absence of any irreversible fouling.

IV.1.2. Experiments in standard conditions

Fig. 3a shows the permeate flux of the water/isopropanol mixtures as a function of the transmembrane pressure (TMP). Except the intercept at zero flux (different from zero only for isopropanol mixtures) this behaviour was similar for each alcohol (see details in **Fig. S3-1 of Supplementary 3**). However, the slope of J_p vs TMP depended of both the alcohol and its content in the water/alcohol mixture as depicted **Fig. 3b**. For a given alcohol, the permeate flux decreased as the alcohol content increased. However, for a given viscosity, fluxes depended on the filtered alcohol as shown **Fig. 3c** (see details in **Fig. S3-1 of Supplementary 3**).

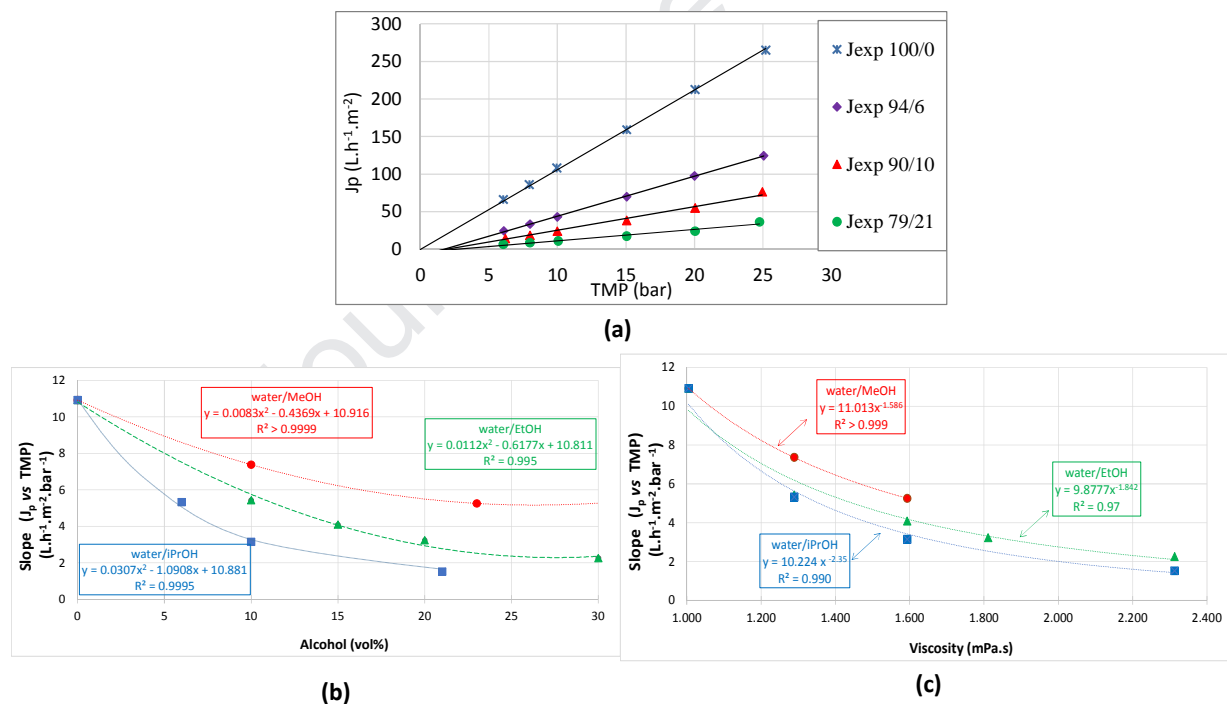


Fig. 3: Experimental flux (J_p) of water/alcohol mixtures during NF in standard conditions - (a) J_p water/isopropanol vs TMP – (b) slope of (J_p vs TMP) vs alcohol content– © slope of (J_p vs TMP) vs viscosity of the water/alcohol mixtures.

IV.2. Rejections

Fig. 4 depicts that experimental rejection of methanol, ethanol and isopropanol increased with flux during NF of the different water/alcohol mixtures.

In the studied flux range the rejection was very different from one alcohol to the other. Methanol rejection remained lower than 8%, that of ethanol lower than 18% and that of isopropanol lower than 50%.

For the lower fluxes, R_{exp} increased roughly linearly with the permeate flux, but the concerned flux range as well as the slope strongly depended on the alcohol (**Fig. 4d**). Unambiguously the rejection order was in good agreement with the alcohol relative V_m : the smaller is the alcohol, the lower was its rejection. It is noticeable that regardless of the BGS viscosity, the alcohol rejection decreased with its Hansen-Hildebrand solubility parameter: the lower is $\delta_{alcohol}$ (**Table 2**) the higher was its rejection.

To tackle the impact of the affinity between the alcohol and the membrane on rejection, the difference between their Hansen-Hildebrand parameters was calculated, knowing that the higher is the affinity the closer are their respective Hansen-Hildebrand parameters. The Hansen-Hildebrand solubility parameter of the membrane was determined by the Fedors method [50]. For this purpose, the unit block of the polypiperazine amide polymer was "cut" into its functional groups and structural fragments. Each group has a cohesion energy (E_{coh_i}) and a molar volume (V_{m_i}) which were found in a referent table [50, 51]. The solubility parameter $\delta_{mb} = 26.2 \text{ (J.cm}^{-3}\text{)}^{1/2}$ was then calculated by addition of contribution of each fragment according to the following equation:

$$\delta = \left(\frac{\sum E_{coh_i}}{\sum V_{m_i}} \right)^{1/2} . \quad (\text{eq. 22})$$

For a given alcohol, R_{exp} varied with J_p . However, the Hansen-Hildebrand parameters of a given alcohol ($\delta_{alcohol}$) or its difference with that of the membrane ($\Delta\delta = \delta_{mb} - \delta_{alcohol}$, commonly expressed in absolute value: $|\Delta\delta|$) were constant meaning that no informative correlations can be found when plotting R_{exp} vs $|\Delta\delta|$. On the contrary the slope of R_{exp} vs J_p was a constant for a given alcohol. Consequently, an attempt of correlation between the average slope of R_{exp} vs J_p and either $\delta_{alcohol}$ or $|\Delta\delta|$ was tested (**Fig. 5**). Thus, a general trend was obtained but it did not really provide a comprehensive explanation of the role of solute-membrane affinity in the rejection: the slope was significantly different for a same solute-membrane affinity as depicted by the absolute value of $\Delta\delta$.

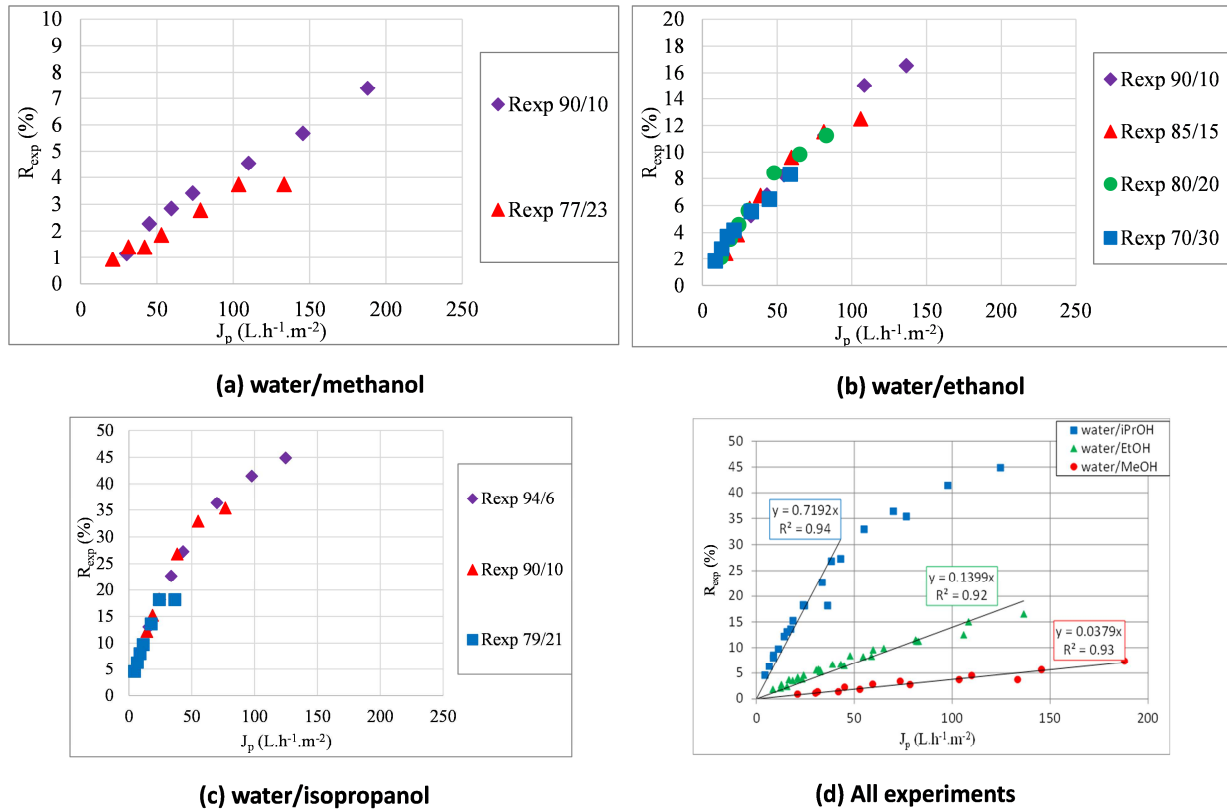


Fig. 4: Experimental Rejections (R_{exp}) of alcohols during NF of water/alcohol mixtures in standard conditions

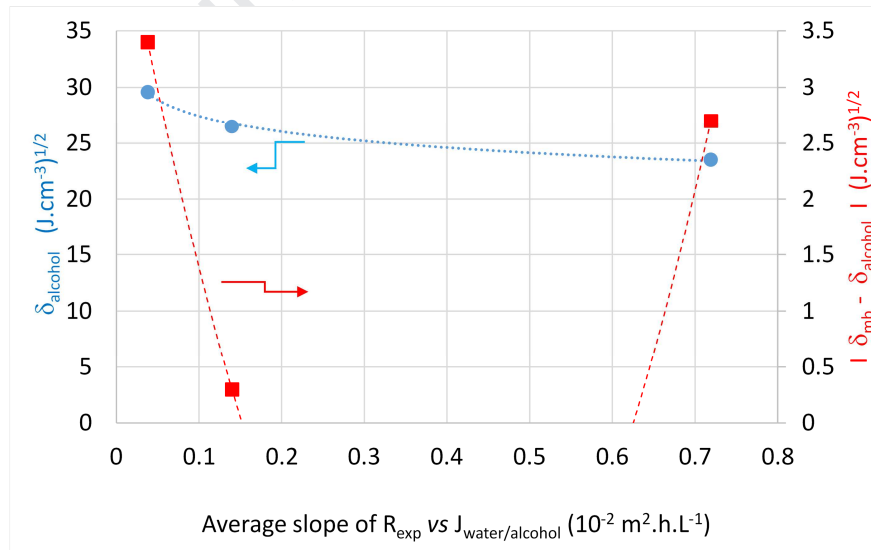


Fig. 5: Attempt of correlation between experimental rejections and Hansen-Hildebrand parameters of alcohol and membrane.

V. Discussion

In this section the modelling of rejection and of mass transfer coefficients are discussed as well as the flux decrease origins.

V.1. Rejection and transfer modelling

V.1.1. Rejections

Fig. 6 shows the results of the modelling with respect to the SD-F approach. At first sight, when only considering the fit quality, the modelling appeared quite nice, especially at lower fluxes for which lot of data were available.

Similarly, **Fig. 7** depicts the results of modelling with respect to the SK-F approach and once again at first sight they seemed to be fitted in a correct way.

To appreciate the real quality of the modelling required to have a look on the fitted parameters (**Table 6 & Table 7**) and on their physical meaning (see the following paragraph).

V.1.2. Mass transfert coefficients

These values were obtained with the Solver of Excel based on the Generalized Reduced gradient (GRC) non-linear method. The derivatives were estimated through forward differencing (default method). The convergence was classically achieved by minimizing the sum of squared residuals. The errors on the 3 fitted parameters were estimated from the experimental errors on rejections, corresponding to that of analyse: ΔR_{exp} . Knowing that the accuracy on rejections was a little better than 10% , calculations were achieved with the maximum $\Delta R_{exp} / R_{exp} = 10\%$ for sake of simplicity. The fitting of a set of experimental data was systematically achieved with R_{exp} , $R_{exp} + \Delta R_{exp}$ and $R_{exp} - \Delta R_{exp}$ to appreciate the maximum and minimum limits of possible results. For instance, the maximum errors when coupling Spiegler&Kedem and Film equations were estimated to 12%, 11% and 12% for k_{SD-F} , σ_{SD-F} and P_{SD-F} , respectively, as an average value for all alcohols. In the case of water/ethanol and water/methanol the accuracy was a little bit better: the maximum errors were estimated to 9%, 11% and 5% for k_{SD-F} , σ_{SD-F} and P_{SD-F} , respectively.

The k_{SD-F} values (**Table 6**) of about 10^{-5} m.s^{-1} has an acceptable physical meaning, thus it could be drawn that it was also the case for δ_{SD-F} . However, the P_{SD-F} represents the solute diffusion in the membrane where no convection occurred and its values were of 10^{-5} m.s^{-1} order. The k_{SD-F} to P_{SD-F} ratio was calculated to easily compare the relative intensity of transfer in the polarization layer and inside the membrane. It seems quite surprising that this ratio could be lower than 1, meaning that the transfer would be easier in the membrane. At first sight it can be drawn that P_{SD-F} values order has no acceptable physical meaning.

The k_{SK-F} values (**Table 7**) of about 10^{-5} $m.s^{-1}$ has also an acceptable physical meaning. According to the SK model, P_{SK-F} represents the solute transfer in the membrane where convection and diffusion could occur. The P_{SK-F} values were of 10^{-5} $m.s^{-1}$ order as for P_{SD-F} just before. But the k_{SK-F} to P_{SK-F} ratio remained higher than 1, in good accordance with an easier transfer in the polarization layer than in the membrane.

Such results suggested that the Solution Diffusion model must be rejected contrary to the Spiegler & Kedem one to describe transfer inside the membrane.

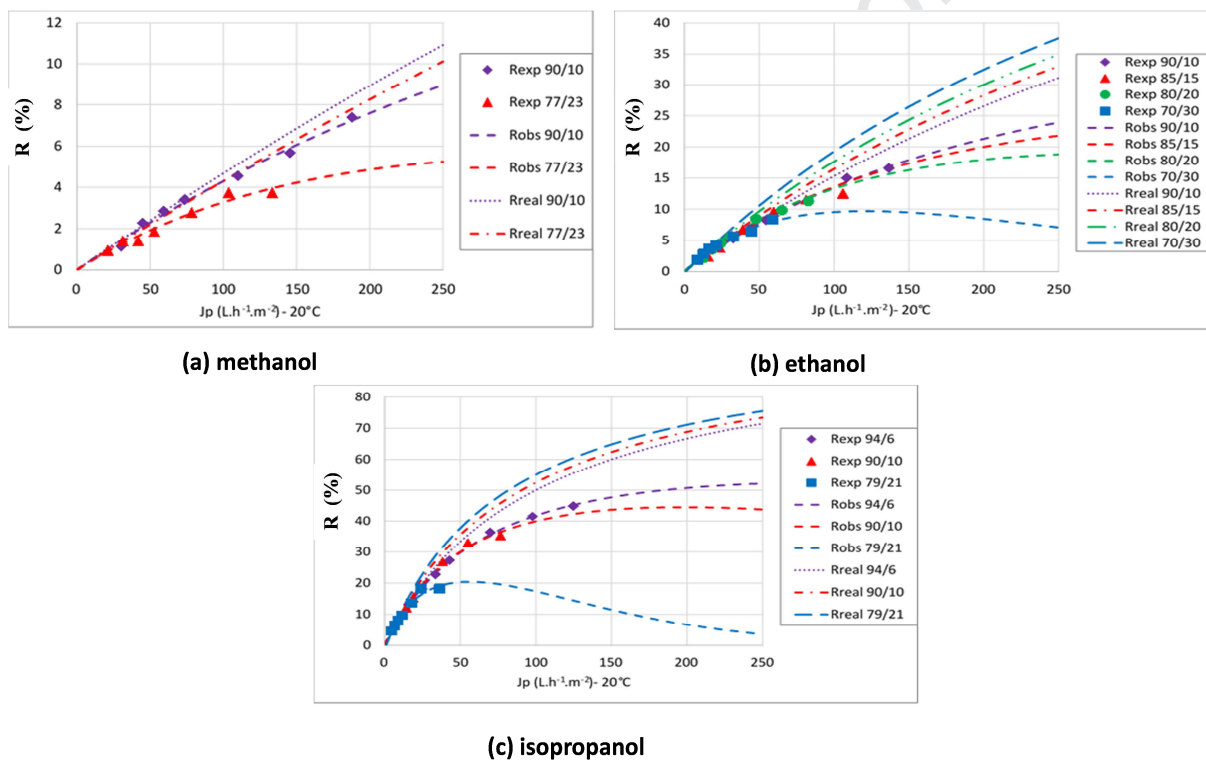


Fig. 6: Modelling of alcohol rejection in water/alcohol mixtures according to the approach coupling solution diffusion and film equations (SD-F).

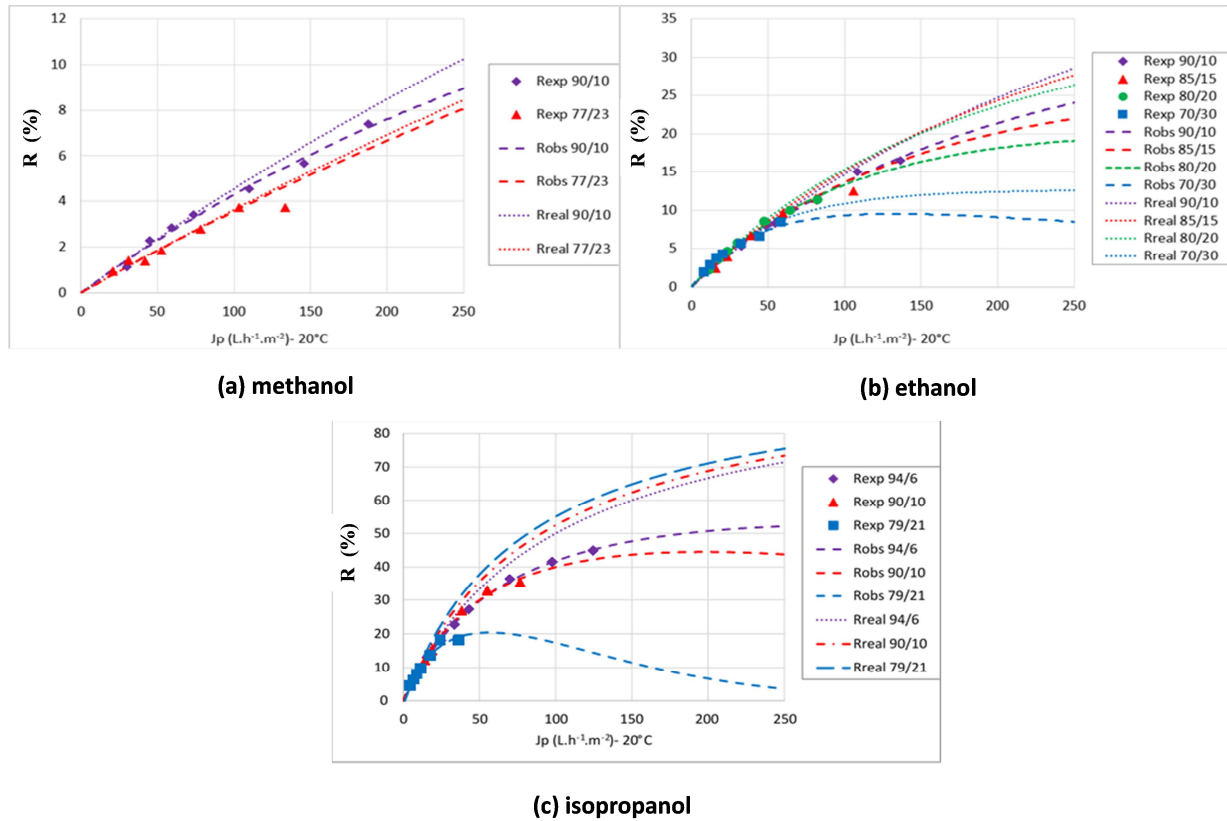


Fig. 7: Modelling of alcohol rejection in water/alcohol mixtures according to the approach coupling Spiegler & Kedem and film equations (**SK-F**).

What about the transport in the polarization layer? The mass transfer coefficient in the polarisation layer deduced from the 2 calculations, k_{SD-F} and k_{SK-F} , exhibited the same trends with respect to the alcohol content: roughly, k decreased with alcohol increase. All values were of the same order, those obtained from SK-F were higher. Taking into account the previous remarks on the physical meaning of P_{SD-F} and P_{SK-F} , it can be assumed that k_{SK-F} would better model the transport in the CP layer than k_{SD-F} . At least the polarization layers were estimated at about 1-2 μm thickness, regardless of the alcohol.

One can notice that the thickness of the polarization layer (further called $\delta_{S\&M}$) can be also estimated from the Sherwood & Michel relation using the Chilton & Colburn analogy involving the Sherwood (Sh), Reynolds (Re) and Schmidt (Sc) dimensionless numbers [52-58]. Detailed calculations are given in **Supplementary 4**. The mass transfer coefficient in the polarisation layer ($k_{S\&M}$) decreased with alcohol increase in good accordance with trends described above. All the 3 values were of the same order, but generally k_{SD-F} and $k_{S\&M}$ were closer than k_{SK-F} and $k_{S\&M}$ (**Fig. S4-1** in **Supplementary 4**). $\delta_{S\&M}$ estimated values were in the 6-8 μm range. Accordingly, the different calculation methods gave values of the polarization layer thickness in

the same order of magnitude but those obtained from SK-F appeared lower than the others (**Fig. S4-1 in Supplementary 4**).

However, the reader must keep in mind that the diffusion coefficients used for these calculations were those in diluted aqueous solutions and probably different from the real values in water/alcohol. For a better accuracy more realistic diffusion coefficients have to be measured. However, having these coefficients in different organic and hydro-organic mixtures remains a major scientific gap that will be difficult to fulfil and time-consuming explaining that it was out of the scope of the present study.

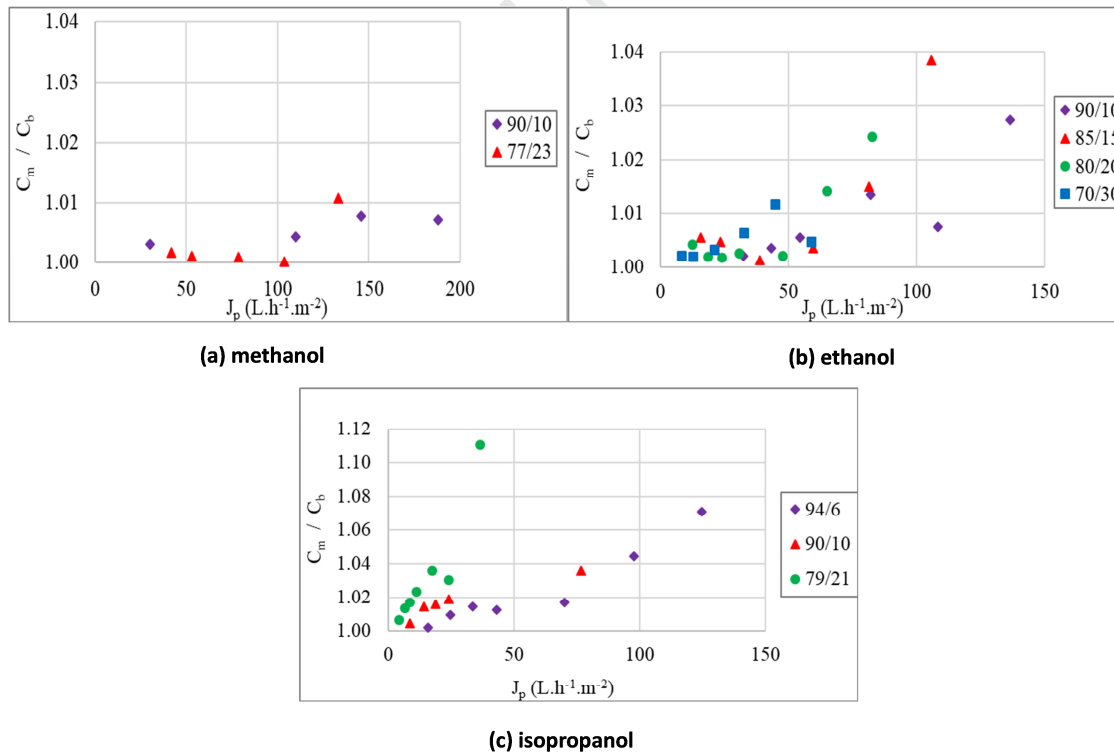
Finally, the C_m values deduced from SK-F were determined from fitted $R_{\text{real,SK-F}}$ values (**Fig. 8**). The polarisation appeared thus really low, whatever the alcohol and will be neglected in the following (in good accordance with preliminary experiments). It can be noticed that similar conclusion can be drawn from SD-F (**Fig. S5-1 in Supplementary 5**) but predicting slightly higher $\delta_{\text{SD-F}}$ and C_m values (**Table 6**).

Table 6: Value of mass transfer coefficients obtained by SD-F model

water/alcohol v/v		$k_{\text{SD-F}}$ ($10^{-5} \cdot \text{m} \cdot \text{s}^{-1}$)	$P_{\text{SD-F}}$ ($10^{-5} \cdot \text{m} \cdot \text{s}^{-1}$)	$k_{\text{SD-F}}/P_{\text{SD-F}}$	$\delta_{\text{SD-F}}$ (μm)
water/	90/10	31	57	0.6	2
methanol	77/23	10	62	0.2	5
	90/10	19	15	1.2	3
water/	85/15	12	14	0.9	4
ethanol	80/20	8	13	0.6	5
	70/30	3	12	0.3	9
water/ isopropanol	94/6	8	3	3.0	5
	90/10	5	3	2.2	6
	79/21	2	2	0.7	7

Table 7: Value of mass transfer coefficients obtained by SK-F model

water/alcohol v/v		k_{SK-F} (10^{-5} m.s^{-1})	P_{SK-F} (10^{-5} m.s^{-1})	k_{SK-F}/P_{SK-F}	σ_{SK-F}	δ_{SK-F} (μm)
water/	90/10	46	26	2	0.46	1
methanol	77/23	36	32	1	0.40	1
	90/10	30	10	3	0.64	2
water/	85/15	23	7	3	0.48	2
ethanol	80/20	17	5	3	0.38	2
	70/30	16	1	12	0.13	2
water/	94/6	25	2	13	0.68	2
isopropanol	90/10	22	1	19	0.51	2
	79/21	22	1	24	0.44	1

**Fig. 8:** C_m/C_b polarisation coefficient during NF of water/alcohol mixtures as calculated according to combination of Spiegler & Kedem and film (SK-F).

V.1.3. Membrane pore size estimation

With respect to the previous conclusion and the validation of the SK-F approach, the membrane pore sizes were determined for each water/alcohol mixtures by coupling SK-F and SHP models.

The membrane pore radius was first estimated using the Stokes radii of alcohols deduced from diffusion experiments in water (given in **Table 2**) by fitting σ_{SHP} and $\sigma_{\text{SK-F}}$ (see **Table S6-2** in **Supplementary 6** for details). It varied between 0.45 and 1.12 nm depending on the water/alcohol mixture. As a general trend, for a given alcohol, the pore radius increased with the alcohol content. In diluted BGS (90/10 water/ethanol and 90/10 water/methanol) the estimated apparent pore radius was about 0.45 nm. This value matched well with those determined in water by the mean of glucose NF in the same filtration conditions, for which we have obtained, $r_{\text{p,water}} = 0.37$ nm (taking $r_{\text{glucose}} = 0.365$ nm) in good accordance with current literature data for NF 270 giving 0.37 nm or 0.43 nm depending on the selected size of glucose that is controversial in literature data [59, 60]. However, we are aware that the determined pore size values were only apparent values because they were not determined with a good accuracy: the solute radii might be different in water and in water/alcohol but data were not available. Their determination is necessary for a better understanding.

However, to overcome this lack of data and reinforce the discussion about the impact of this critical parameter, several others assumptions were tested dealing with the alcohol radius values. They were inspired by the approach reported by van der Bruggen *et al.* [40] where 3 different size were considered for alcohols either based on Stokes radius ($r_{\text{s,Stokes}}$, valid in diluted aqueous solutions), equivalent molar radius calculated from the molar volume (valid in pure alcohols and hereafter noted $r_{\text{s,Vm}}$) and a third one based on theoretical calculations and further called theoretical molecular radius and noted $r_{\text{s,theoretical}}$. The calculation mode of $r_{\text{s,theoretical}}$ based on an energetic optimisation procedure was reported in [40] as an iterative procedure using the computer program HyperChem based on [61] the molecular energy being minimised by adjusting the configuration of the molecule. These solute radii values are given in **Table 8** (see also **Table S6-1** in **Supplementary S6-1**).

Then adjusting σ_{SHP} to $\sigma_{\text{SK-F}}$ using the different assumption on the solute radii allowed to calculate a set of membrane pore radii for all BGS filtrations (**Table 8**, see also **Fig. S6-1** in **Supplementary 6**). Finally, we decided to test a last approach: the adjustment between σ_{SHP} to $\sigma_{\text{SK-F}}$ was made by using the excel solver ability to found the best fit by adjusting simultaneously the two radii, r_{s} and r_{p} . Knowing that r_{s} is lower than r_{p} in water and assuming that it would be the same in water/alcohol, then we have used the following constraint $r_{\text{s}} < r_{\text{p}}$ to accelerate the convergence of the results and avoid results with non-physical meaning. The results were hereafter noted simultaneously adjusted r_{s} or r_{p} , respectively (**Table 8**, see also **Fig. S6-2** in **Supplementary 6**). Depending on the alcohol the adjusted solute radius can be closer to one or the other assumption and we are not able to explain why. Regardless the assumption on the

solute radius, the membrane pore radius tended to increase with the alcohol content in good agreement with an expected swelling.

Table 8: Solute and pore radii (in nm) according to different assumptions

Alcohol vol%	$r_{s,Stokes}$	$r_{p,Stokes}$	$r_{s,Vm}$	$r_{p,Vm}$	$r_{s,theoretical}$	$r_{p,theoretical}$	simultaneously adjusted rs	simultaneously adjusted r_p
MeOH								
10	0.26	0.46	0.26	0.46	0.21	0.37	0.28	0.50
23	0.26	0.48	0.26	0.48	0.21	0.40	0.29	0.55
EtOH								
10	0.31	0.46	0.29	0.43	0.26	0.38	0.32	0.47
15	0.31	0.54	0.29	0.50	0.26	0.45	0.30	0.52
20	0.31	0.61	0.29	0.57	0.26	0.51	0.29	0.56
30	0.31	1.08	0.29	1.01	0.26	0.91	0.22	0.75
i-PrOH								
6	0.40	0.57	0.31	0.44	0.29	0.41	0.30	0.43
10	0.40	0.67	0.31	0.52	0.29	0.49	0.28	0.48
21	0.40	0.73	0.31	0.56	0.29	0.53	0.29	0.52

Fig. 9 depicts attempts of correlation between physico-chemical parameters of the water/alcohol mixtures (**Table 3**) and the pore radius according to the several assumptions (**Table 8**).

Fig. 9a shows that the apparent pore size increased with the increase in the BGS/membrane affinity (lower difference between the Hansen Hildebrand parameters).

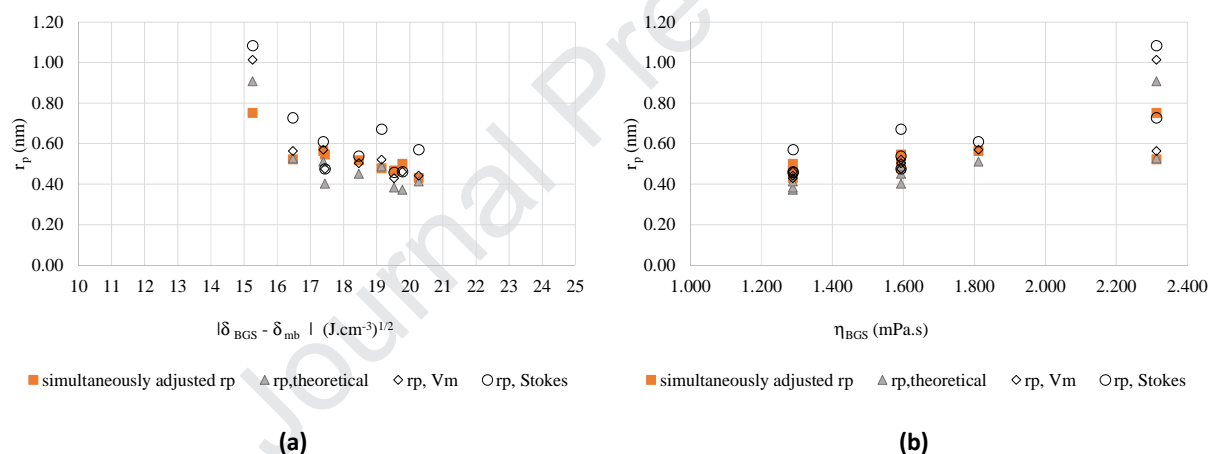
Fig. 9b also suggests a strong impact of the BGS viscosity. Supporting this observation, **Table 9** depicts the average apparent pore radius calculated as the mean of all pore radius obtained for a given viscosity, regardless of other assumptions. The precision was better than 13% for all values except that obtained at the higher viscosity.

More or less the membrane pore could be considered as roughly constant for viscosity lower than 1.9 mPa.s: the average value was $r_p = 0.50 \pm 0.07$ nm highlighting a little impact of the membrane swelling (**Table 9**).

For the highest viscosity (2.313 mPa.s) also corresponding to the highest alcohol contents, the balance between the viscosity and the affinity evolved and the membrane pore depended more strongly on the alcohol chemical nature in good agreement with **Fig. 9a**.

Table 9: Estimation of average apparent pore radius for a given viscosity regardless of the alcohol

Viscosity of water/alcohol mixture (mPa.s)	r_p , average (nm)
1.289	0.45 ± 0.06
1.593	0.51 ± 0.07
1.811	0.56 ± 0.04
2.313	0.76 ± 0.22
Average except 2.313 mPa.s	0.50 ± 0.07

**Fig. 9:** Attempt of correlation between physico-chemical parameters of the water/alcohol mixtures (Table 3) and the apparent pore radius (see also Fig. S6-1 in supplementary 6).

V.2. Flux decrease origin

Besides the above pore size calculation, a second approach is now discussed based on the membrane hydraulic resistance experimental determination. The dissolution, deformation or swelling of organic NF membranes can significantly affect their performances [62, 63]. Indeed, the movement of polymer chains (closer or farer) could change the free volumes which affects the solvent transfer. Accordingly, the hydraulic resistance of the membrane would depend on the solvent-membrane affinity.

Alcohols have better affinity towards the polypiperazineamide membrane than water as it can be evidenced from the difference in their Hansen-Hildebrand parameters (**Table 3, [64]**). However, the main question at start remained the swelling limitation with respect to the (unknown) cross-linking rate of the polymer but suggested by the pore radius increase (see above). To underline possible changes, the membrane hydraulic resistance in water was hereafter noticed $R_{m,water}$ whereas that in water/alcohol was noticed $R_{m,BGS}$.

The following discussion required to also appreciate the impact of the difference in osmotic pressure assuming a negligible impact of concentration polarisation that has been demonstrated above as well as the absence of irreversible fouling.

V.2.1. Osmotic pressure difference and membrane resistance determination

Following the overall approach exposed in the theoretical section, the difference in osmotic pressure ($\Delta\pi_{obs} = \pi_{bulk} - \pi_{permeate}$) were calculated from alcohol experimental rejections (**Figure 4**) and following the different assumptions on B' (**eq. 17**). Variation of the viscosity between the retentate and the permeate due to the alcohol rejection has been taken into account.

For all NF experiments, the calculated permeate flux (**eq. 16**) was adjusted to the experimental one using $R_{m,BGS}$ as adjusting parameter, allowing thus its determination. Of course following this approach assumed that $R_{m,BGS}$ was constant with TMP for a given BGS. This assumption will be discussed in the following with respect to the obtained standard deviations. **Table 10** sums up the average values of $R_{m,BGS}$.

○ Ethanol

Depending on the ethanol concentration, $\Delta\pi_{obs}$ varied between 0 and 12 bar (see also **Fig. S7-1** in **Supplementary 7**). Regardless of the assumption $\Delta\pi_0$ at zero flux was lower than 4 bar in good agreement with experimental data (see also **Fig. S3-1b** in **Supplementary 3**, intercept of the straight lines at zero flux). Adjusted $R_{m, BGS}$ are shown **Fig. 10a** (see also **Fig. S7-2** in **Supplementary 7** to check the good quality of adjustment). On the whole ethanol range (0-30 vol%) $R_{m,BGS}$ was evidenced to only vary within a relative standard deviation of 7.5% (including pure water). The average resistance was $R_{m,BGS} = (3.6 \pm 0.3) \times 10^{13} \text{ m}^{-1}$.

○ Methanol

Depending on the methanol concentration, $\Delta\pi_{obs}$ varied between 0.5 and 6 bar (**Fig. S8-1** in **Supplementary 8**). Regardless of the assumption $\Delta\pi_0$ was less than 4 bar in good agreement with experimental data (see also **Fig. S3-1c** in **Supplementary 3**). Adjusted $R_{m, BGS}$ are shown **Fig.10b** (see also **Fig. S9-2** in **Supplementary 9** to check the good quality of adjustment). On the whole methanol range (0-23 vol%), $R_{m,BGS}$ was evidenced to only vary within a relative standard deviation of 3% (including pure water). The average resistance was $R_{m,BGS} = (3.24 \pm 0.01) \times 10^{13} \text{ m}^{-1}$. This is in a rather good agreement with conclusions drawn about the pore size (**Table 8**).

○ Isopropanol

Depending on the isopropanol concentration, $\Delta\pi_{obs}$ varied between 2.5 and 14 bar (see also **Fig. S9-1** in **Supplementary 9**). Regardless of the assumption $\Delta\pi_0$ was less than 4 bar in good

agreement with experimental data of **Fig. 3a**. Adjusted $R_{m, BGS}$ are shown **Fig.10c** (see also **Fig. S9-2** in **Supplementary 9** to check the good quality of adjustment). The average resistance was $R_{m, BGS} = (4.3 \pm 0.9) \times 10^{13} \text{ m}^{-1}$ corresponding to a relative standard deviation of 22% highlighting that it cannot be considered as a constant value over the whole range. On the whole isopropanol range (0-21 vol%), $R_{m, BGS}$ was evidenced to regularly increase.

Table 10: $R_{m, water}$ and average $R_{m, BGS}$ for the different water/alcohol mixtures

Alcohol range (%)	water	water/MeOH	water/EtOH		water/i-PrOH	
	0	0-23	0-30	10-30	0-21	6-10
Viscosity range (mPa.s)	1.000	1.000-1.593	1.000-2.313	1.289 – 2.313	1.000-2.313	1.000-1.593
$R_{m, water}$ or $R_{m, BGS}$ (10^{13} m^{-1})	3.19 ± 0.07	3.24 ± 0.01	3.6 ± 0.3	3.7 ± 0.2	4.3 ± 0.9	4.2 ± 0.4
RSD (%)	2.0	3.0	7.5	5.1	22	8.6

Finally, regardless of the alcohol, the relative stability of $R_{m, BGS}$ was in good agreement with conclusions drawn about the pore size stability at lower alcohol contents. However, for the higher alcohol amounts (EtOH, i-PrOH) the increase in $R_{m, BGS}$ appeared at first sight in full contradiction with the increase of pore size (**Table 8**). This will be discussed in the following paragraph.

V.2.2. Membrane swelling along different directions

The previous calculations underlined that the membrane resistance could sometimes increase simultaneously with the pore size, thus an insight in the origin of the resistance possible variation must be discussed now. When considering a porous membrane, the following Hagen-Poiseuille equation highlights that a significant swelling might lead to an increase of the pore radius together with an increase of the membrane thickness (Δx).

$$J_p = \text{TMP} \frac{r_p^2}{8 \eta \left(\frac{\Delta x}{A_k} \right)} \quad (\text{eq. 23})$$

With:

Δx : the membrane thickness

A_k : the membrane porosity

Eq. 23 can be rewritten according to the following one allowing the determination of the $\Delta x/A_k$ ratio variation using the $R_{m,BGS}$ and pore radii described above:

$$R_m = \frac{8}{r_p^2} \left(\frac{\Delta x}{A_k} \right) \quad (\text{eq. 24})$$

As more or less, all assumptions on the alcohol solute size and on B' led to the same trends, for sake of simplification we only discussed the case for which both the solute radius and the pore radius were simultaneously adjusted (**Table 8**). $R_{m,BGS}$ used in calculations were selected as those corresponding to $B' = V_m$ because all flux adjustments were of good quality (see also **Fig. S7-2**, **Fig. S8-2**, **Fig. S9-2** in **Supplementary 7-9**).

Fig. 11 depicts that the $\Delta x/A_k$ ratio increased with the alcohol content, so simultaneously with the pore size increase and the alcohol affinity for the membrane. This means that the swelling also impacted the membrane thickness. Finally, at low alcohol contents the slight increase of both the membrane thickness and the pore were compensated leading to an unexpected roughly stable membrane resistance. At high alcohol amount, the membrane thickness increase impact overcame that of the pore radius increase.

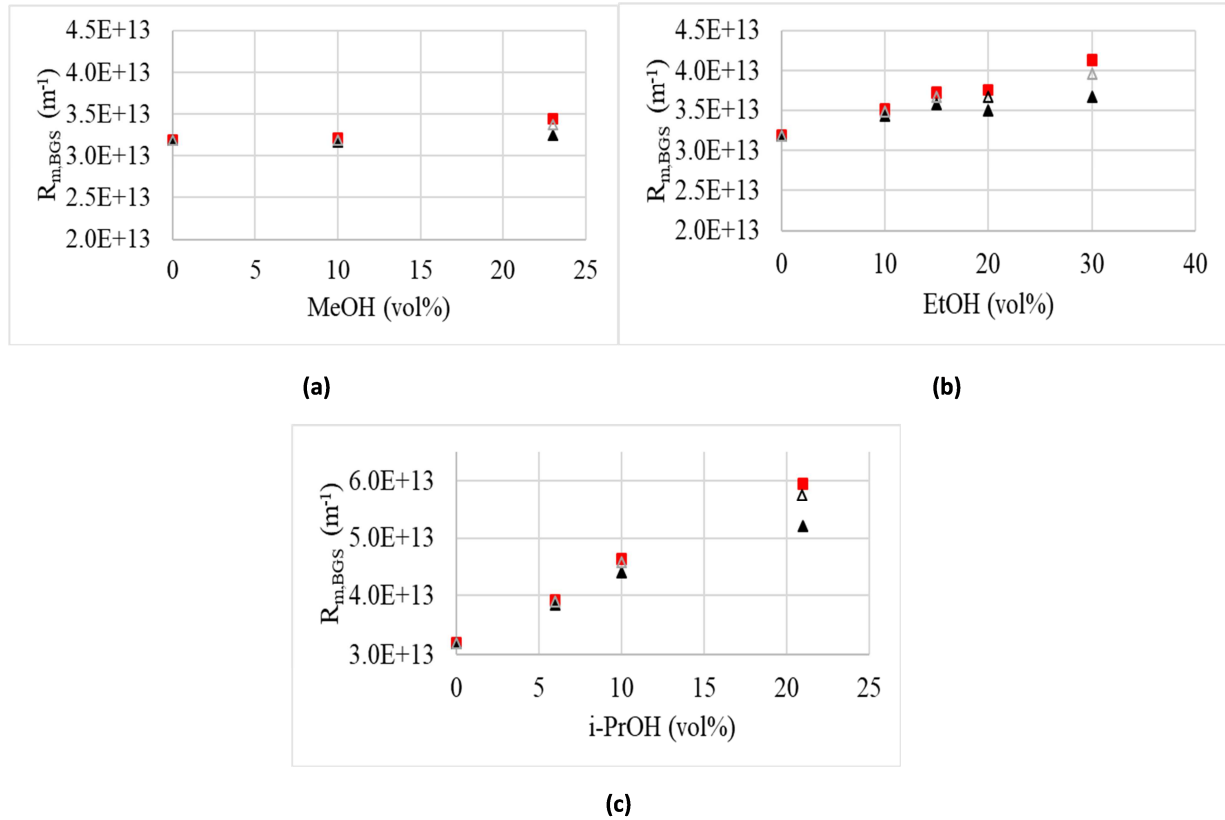


Fig. 10: Membrane resistance in water ($R_{m,water}$) and water/alcohol ($R_{m,BGS}$) calculated from $\Delta\pi_{obs}$, according to assumption on B' in virial expansion (see **Table 4**): ■: van't Hoff, ▲: $B' = V_m$, △: $B' = V_{m,BGS}$

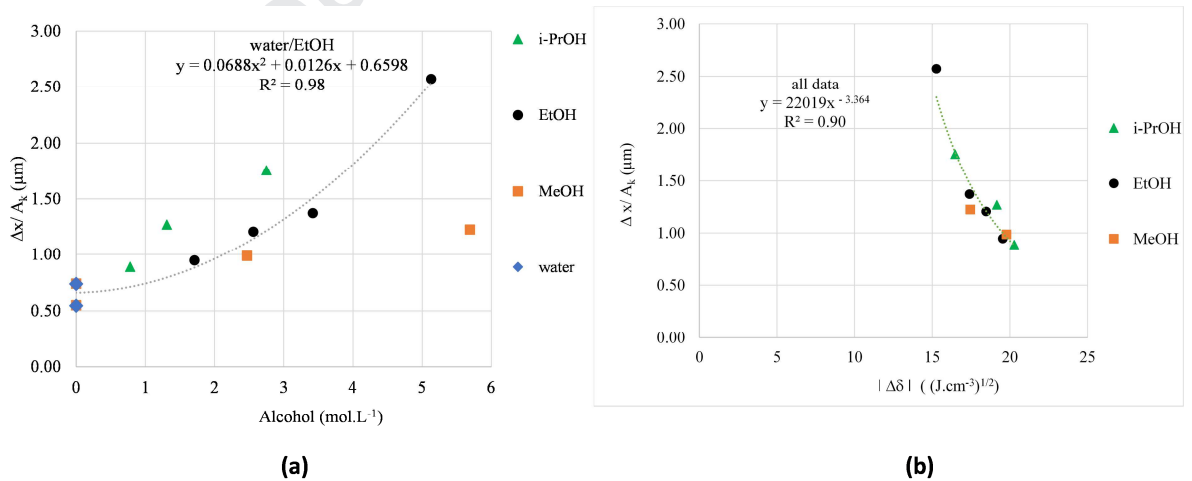


Fig. 11: the $\Delta x/A_k$ ratio variation determined from **eq. 24**, using the $R_{m,BGS}$ value for $B'=V_m$ (**Fig. 10**) and membrane pore radius of **Table 8** (simultaneously determined value)

VI. Conclusion

The three alcohols selected for this study, methanol, ethanol and isopropanol, exhibit different physico-chemical characteristics among which are: size, hydrophobicity, Hansen-Hildebrand solubility parameters. NF with NF 270 polypiperazine amide membrane (Dow Filmtec) was achieved for several water/alcohol compositions allowing a significant variation of the viscosity up to about twice that of water with respect to alcohol contents.

Regardless of the alcohols, that were shown to be partly retained by the membrane, the flux in water/alcohol significantly decreased when compared to that in water. Contrary to solution diffusion, by using the Spiegler & Kedem approach coupled with the Film Theory the experimental rejections of alcohol were modelled in a satisfying way and the transfer coefficients either in the bulk or in the membrane were determined.

The pore radius was estimated by coupling Spiegler & Kedem and film equations together with the Steric Hindrance Pore model and applied to the alcohols considered as acting as (1) neutral solutes and (2) as modifier of the viscosity of the background solvent. Several assumptions were tested dealing with the alcohol radii in water/alcohol mixtures but more or less all assumptions led to the same conclusion: compared to water, the membrane pore size was not significantly changed at low alcohol content but increased at high ethanol (30 vol%) and isopropanol (21 vol%) amounts.

The flux behaviour was fairly good modelled by considering a constant hydraulic resistance of the membrane for a given water/alcohol mixture ($R_{m,BGS}$) and the combination of the viscosity increase and of the osmotic pressure difference calculated by using the first coefficient virial expansion as alcohol concentration was sometimes greater than 1 mol.L^{-1} . Surprisingly, the membrane resistance was roughly constant at the lower alcohol amount and close to that in water. However, it increased at high amount of ethanol (30 vol%) and isopropanol (21 vol%) highlighting that in these last cases the pore size increase (leading to a decrease in resistance) was overcome by the increase in the membrane thickness (leading to an increase in resistance) both being the consequence of the membrane swelling in presence of the organic solute at sufficient concentration.

Acknowledgements

Thi Vi Na NGUYEN acknowledges the French Ministry of Research for the financial support of her PhD grant.

Lists of symbols

BGS	Background solvent (water/alcohol mixture)
C _b	Concentration in bulk retentate
C _i	Concentration solute i
C _m	Concentration at membrane wall
CP	Concentration polarisation
C _p	Concentration in permeate
Δe	Membrane thickness
D _i	Diffusion coefficient of solute i
J _p	Permeate volume flux
k	Mass transfert coefficient in film model
k _B	Boltzmann constant
k _{SD-F}	Mass transfert coefficient in Solution-Diffusion & film model
k _{SK-F}	Mass transfert coefficient in Spiegler-Kedem & film model
L _p	Membrane permeance
MWCO	Molecular Weigth Cut Off
N _A	Avogadro number ($N_A = 6.022 \cdot 10^{23} \text{ mol}^{-1}$)
NF	Nanofiltration
OSN	Organic Solvent Nanofiltration
PDMS	Polydimethylsiloxane
P _{SD}	Solute permeability in solution-diffusion model
P _{SD-F}	Solute permeability in solution-diffusion model coupled with film theory
P _{SK}	Solute permeability in Spiegler & Kedem model
P _{SK-F}	Solute permeability in Spiegler & Kedem model coupled with film theory
R _(gas)	Gas constant ($R=8.314 \text{ J} \cdot \text{mol}^{-1} \cdot \text{K}^{-1}$)
R	Rejection
R _{exp}	Experimental rejection
R _{obs}	Observed rejection
R _{real}	Real rejection
R _m	Membrane hydraulic resistance
R _{m,water}	Membrane hydraulic resistance in water

$R_{m,BGS}$	Membrane hydraulic resistance in BGS
r_p	Membrane pore radius
$r_{p,Stokes}$	Membrane pore radius calculated from $r_{s,Stokes}$ in water
$r_{p,theoretical}$	Membrane pore radius calculated from theoretical approach
r_{p,V_m}	Membrane pore radius calculated from V_m (pure alcohol)
r_s	radius of solute
$r_{s,Stokes}$	Stokes radius of solute (in water)
r_{s,V_m}	radius of solute in BGS calculated from $V_{m,BGS}$
$r_{s,theoretical}$	solute radius calculated from theoretical approach
SD	Solution-Diffusion model
SD-F	Solution-Diffusion & Film model
SHP	Steric-Hindrance Pore model
SK	Spiegler-Kedem model
SK-F	Spiegler-Kedem & Film model
TMP	Transmembrane pressure
v	cross-flow velocity
V_m	Molar volume of alcohol in pure alcohol
$V_{m,BGS}$	Average molar volume of alcohol in BGS
x_i	Molar fraction of solute i

Greek symbols

A_k	Membrane porosity
δ_{CP}	Polarisation layer thickness
δ_i	Solubility parameter of solute i
ϵ_r	Dielectric constant
π_i	Osmotic pressure
π_{virial}	Osmotic pressure calculated with the virial assumption
σ_i	Reflexion coefficient of solute i
σ_{SK-F}	Reflexion coefficient of solute i calculated from SK-F combination

σ_{SHP}	Reflexion coefficient of solute <i>i</i> calculated from SHP model
$\Delta\pi$	Osmotic pressure difference
η	Viscosity

References

- 1 P.T. Anastas, J.C. Warner, *Green Chemistry: Theory and Practice*, Oxford University Press, New York, 1998.
- 2 C.G. Lopresto, S. Darvishmanesh, A. Ehsanzadeh, A. Amelio, S. Mazinani, R. Ramazani, V. Calabrò, B. Van der Bruggen, Application of organic solvent nanofiltration for microalgae extract concentration: Solvent separation by nanofiltration, *Biofuels, Bioproducts Biorefining*. 11 (2017) 307–324. doi:10.1002/bbb.1738.
- 3 B.C.B.S. Mello, J.C.C. Petrus, M.D. Hubinger, Concentration of flavonoids and phenolic compounds in aqueous and ethanolic propolis extracts through nanofiltration, *J. Food Eng.* 96 (2010) 533–539. doi:10.1016/j.jfoodeng.2009.08.040.
- 4 F. Salehi, Current and future applications for nanofiltration technology in the food processing, *Food Bioproducts Process.* 92 (2014) 161–177. doi:10.1016/j.fbp.2013.09.005.
- 5 A.W. Mohammad, Y.H. Teow, W.L. Ang, Y.T. Chung, D.L. Oatley-Radcliffe, N. Hilal, Nanofiltration membranes review: Recent advances and future prospects, *Desalination*. 356 (2015) 226–254. doi:10.1016/j.desal.2014.10.043.
- 6 W.R. Bowen, A.W. Mohammad, N. Hilal, Characterisation of nanofiltration membranes for predictive purposes ? use of salts, uncharged solutes and atomic force microscopy, *J. Membrane Sci.* 126 (1997) 91–105. doi:10.1016/S0376-7388(96)00276-1.
- 7 T. Tsuru, S. Nakao, S. Kimura, Calculation of ion rejection by extended Nernst-Planck equation with charged reverse osmosis membranes for single and mixed electrolyte solutions, *J. Chem. Eng. Japan*. 24 (1991) 511–517. doi:10.1252/jcej.24.511.
- 8 P. Marchetti, M.F. Jimenez Solomon, G. Szekely, A.G. Livingston, Molecular Separation with Organic Solvent Nanofiltration: A Critical Review, *Chem. Rev.* 114 (2014) 10735–10806. doi:10.1021/cr500006j.
- 9 M. Cissé, F. Vaillant, D. Pallet, M. Dornier, Selecting ultrafiltration and nanofiltration membranes to concentrate anthocyanins from roselle extract (*Hibiscus sabdariffa* L.), *Food Res. Inter.* 44 (2011) 2607–2614. doi:10.1016/j.foodres.2011.04.046.
- 10 A. Giacobbo, A.M. Bernardes, M.N. de Pinho, Nanofiltration for the Recovery of Low Molecular Weight Polysaccharides and Polyphenols from Winery Effluents, *Sep. Sci. Technol.* 48 (2013) 2524–2530. doi:10.1080/01496395.2013.809762.

- 11 I.H. Tsibranska, B. Tylkowski, Concentration of ethanolic extracts from *Sideritis* ssp. L. by nanofiltration: Comparison of dead-end and cross-flow modes, *Food Bioproducts Process.* 91 (2013) 169–174. doi:10.1016/j.fbp.2012.09.004.
- 12 E.M. Tsui, M. Cheryan, Membrane processing of xanthophylls in ethanol extracts of corn, *J. Food Eng.* 83 (2007) 590–595. doi:10.1016/j.jfoodeng.2007.03.041.
- 13 D. Peshev, L.G. Peeva, G. Peev, I.I.R. Baptista, A.T. Boam, Application of organic solvent nanofiltration for concentration of antioxidant extracts of rosemary (*Rosmarinus officinalis* L.), *Chem. Eng. Res. Design.* 89 (2011) 318–327. doi:10.1016/j.cherd.2010.07.002.
- 14 B. Tylkowski, B. Trusheva, V. Bankova, M. Giamberini, G. Peev, A. Nikolova, Extraction of biologically active compounds from propolis and concentration of extract by nanofiltration, *J. Membrane Sci.* 348 (2010) 124–130. doi:10.1016/j.memsci.2009.10.049.
- 15 M. Bastin, J. Raymenants, Y. Vankelecom, Epoxy-based SRNF membranes prepared through phase inversion, oral communication at OSN 2019, 28-31 octobere, 2019, Enschede (NL)
- 16 P. Marchetti, A. Butté, A.G. Livingston, An improved phenomenological model for prediction of solvent permeation through ceramic NF and UF membranes, *J. Membrane Sci.* 415–416 (2012) 444–458. doi:10.1016/j.memsci.2012.05.030.
- 17 A. Buekenhoudt, F. Bisignano, G. De Luca, P. Vandezande, M. Wouters, K. Verhulst, Unravelling the solvent flux behaviour of ceramic nanofiltration and ultrafiltration membranes, *J. Membrane Sci.* 439 (2013) 36–47. doi:10.1016/j.memsci.2013.03.032.
- 18 A. Volkov, A. Yushkin, A. Grekhov, A. Shutova, S. Bazhenov, S. Tsarkov, V. Khotimsky, T.J.H. Vlught, V. Volkov, Liquid permeation through PTMSP: One polymer for two different membrane applications, *J. Membrane Sci.* 440 (2013) 98–107. doi:10.1016/j.memsci.2013.03.067.
- 19 J. Geens, K. Peeters, B. Vanderbruggen, C. Vandecasteele, Polymeric nanofiltration of binary water–alcohol mixtures: Influence of feed composition and membrane properties on permeability and rejection, *J. Membrane Sci.* 255 (2005) 255–264. doi:10.1016/j.memsci.2005.01.039.
- 20 J. Labanda, J. Sabaté, J. Llorens, Permeation of organic solutes in water–ethanol mixtures with nanofiltration membranes, *Desalination.* 315 (2013) 83–90. doi:10.1016/j.desal.2012.10.007.
- 21 E. Tsui, Characteristics of nanofiltration membranes in aqueous ethanol, *J. Membrane Sci.* 237 (2004) 61–69. doi:10.1016/j.memsci.2004.02.026.
- 22 J. Luo, L. Ding, X. Chen, Y. Wan, Desalination of soy sauce by nanofiltration, *Sep. Purif. Technol.* 66 (2009) 429–437.
- 23 L.A. Richards, the removal of inorganic contaminants using nanofiltration and reverse osmosis, PhD thesis report (2012) Heriot-Watt University, UK
- 24 B. González, N. Calvar, E. Gómez, Á. Domínguez, Density, dynamic viscosity, and

- derived properties of binary mixtures of methanol or ethanol with water, ethyl acetate, and methyl acetate at $T=(293.15, 298.15, \text{ and } 303.15)\text{K}$, *J. Chem. Thermo.* 39 (2007) 1578–1588. doi:10.1016/j.jct.2007.05.004.
- 25 F.-M. Pang, C.-E. Seng, T.-T. Teng, M.H. Ibrahim, Densities and viscosities of aqueous solutions of 1-propanol and 2-propanol at temperatures from 293.15 K to 333.15 K, *J. Mol. Liq.* 136 (2007) 71–78. doi:10.1016/j.molliq.2007.01.003.
- 26 I.S. Khattab, F. Bandarkar, M.A.A. Fakhree, A. Jouyban, Density, viscosity, and surface tension of water+ethanol mixtures from 293 to 323K, *Korean J. Chem. Eng.* 29 (2012) 812–817. doi:10.1007/s11814-011-0239-6.
- 27 G. Akerlof, Dielectric constants of some organic solvent-water mixtures at various temperatures., *J. Am. Chem. Soc.* 54 (1932) 4125–4139.
- 28 G. Schock, A. Miquel, Mass transfer and pressure loss in spiral wound modules, *Desalination.* 64 (1987) 339–352. doi:10.1016/0011-9164(87)90107-X.
- 29 A. Bouchoux, H. Roux-de Balman, F. Lutin, Nanofiltration of glucose and sodium lactate solutions : variations of retention between single- and mixed-solute solutions, *J. Membrane Sci.* 258 (2005) 123–132. doi:10.1016/j.memsci.2005.03.002.
- 30 J.G. Wijmans, R.W. Baker, The solution-diffusion model: a review, *J. Membrane Sci.* 107 (1995) 1–21. doi:10.1016/0376-7388(95)00102-I.
- 31 Z.V.P. Murthy, S.K. Gupta, Estimation of mass transfer coefficient using a combined nonlinear membrane transport and film theory model, *Desalination.* 109 (1997) 39–49. doi:10.1016/S0011-9164(97)00051-9.
- 32 K.S. Spiegler, O. Kedem, Thermodynamics of hyperfiltration (reverse osmosis): criteria for efficient membranes, *Desalination* 101 (1966) 311-326.
- 33 S.-I. Nakao, S. Kimura, Models of membrane transport phenomena and their applications for ultrafiltration data., *J. Chem. Eng. Japan.* 15 (1982) 200–205. doi:10.1252/jcej.15.200.
- 34 <http://ddbonline.ddbst.de/UNIFACCcalculation/UNIFACCcalculationCGI.exe?component1=Ethanol&component2=Water&temperatures=298&calculate=Calculate>
- 35 P.C. Hiemenz, R. Rajagopalan (Eds.), *Principles of Colloid and Surface Chemistry*, 3rd edition Marcel Dekker, New York, 1997, p. 114.
- 36 A. D. Jenkins, J. F. Kennedy and J. W. Kennedy, Chap. 14: Thermodynamics of solutions and mixtures, Pages 296 - 330 in *Macromolecular Chemistry: Volume 1* Editors: A D Jenkins, John F Kennedy, Royal Society of Chemistry, 1980, London, doi:10.1039/9781847556554-FX001
- 37 Y.U. Moon, C.O. Anderson, H.W. Blanch, J.M. Prausnitz, Osmotic pressures and second virial coefficients for aqueous saline solutions of lysozyme, *Fluid Phase equilibria*, 168, 2000, 229-239. [https://doi.org/10.1016/S0378-3812\(99\)00337-4](https://doi.org/10.1016/S0378-3812(99)00337-4)

- 38 X. Ge, X. Wang, M. Zhang, S. Seetharaman. Correlation and Prediction of Activity and Osmotic Coefficients of Aqueous Electrolytes at 298.15 K by the Modified TCPC Model. *J. Chem. Eng. data.* 52 (2007) 538-547.
- 39 X. Ge, M. Zhang, M. Guo, X. Wang, Correlation and Prediction of Thermodynamic Properties of Non-aqueous Electrolytes by the Modified TCPC Model. *J. Chem. Eng. data.* 53 (2008)149-159.
- 40 B. Van der Bruggen, J. Schaep, D. Wilms, C. Vandecasteele, Influence of molecular size, polarity and charge on the retention of organic molecules by nanofiltration, *J. Membrane Sci.* 156 (1999) 29–41. doi:10.1016/S0376-7388(98)00326-3.
- 41 <https://wissen.science-and-fun.de/chemistry/chemistry/density-tables/ethanol-water-mixtures/>
- 42 D.R. Machado, D. Hasson, R. Semiat, Effect of solvent properties on permeate flow through nanofiltration membranes. Part I: investigation of parameters affecting solvent flux, *J. Membrane Sci.* 163 (1999) 93–102. doi:10.1016/S0376-7388(99)00158-1.
- 43 I.S.Khattab, F. Bandarkar, M.A.A. Fakhree, A. Jouyban, Density, viscosity, and surface tension of water+ethanol mixtures from 293 to 323 K, *Korean J ; Chem. Eng.* 29 (2012) 812-817. doi : 10.1007/s1184-011-0239-6
- 44 S.Z. Mikhail and W.R. Kimel, Densities and Viscosities of Methanol-Water Mixtures, *J. Chem. Eng. Data* 6 (1961)
- 45 V.I. Kuchuk, I. Yu. Shirokova, E. V. Golikova, Physicochemical properties of water-alcohol mixtures of a homological series of lower aliphatic alcohols, *Glass Phys. Chem.* 38 (2012) 460–465
- 46 P. Vandezande, X. Li, L.E.M. Gevers, I.F.J. Vankelecom, High throughput study of phase inversion parameters for polyimide-based SRNF membranes, *J. Membrane Sci.* 330 (2009) 307–318. doi:10.1016/j.memsci.2008.12.068.
- 47 I. Soroko, M.P. Lopes, A. Livingston, The effect of membrane formation parameters on performance of polyimide membranes for organic solvent nanofiltration (OSN): Part A. Effect of polymer/solvent/non-solvent system choice, *J. Membrane Sci.* 381 (2011) 152–162. doi:10.1016/j.memsci.2011.07.027.
- 48 S. Romero, Solubility behavior of polymorphs I and II of mefenamic acid in solvent mixtures, *Inter. J. Pharma.* 178 (1999) 193–202. doi:10.1016/S0378-5173(98)00375-5.
- 49 D. Bhanushali, S. Kloos, C. Kurth, D. Bhattacharyya, Performance of solvent-resistant membranes for non-aqueous systems: solvent permeation results and modelling, *J. Membrane Sci.* 189 (2001) 1–21. doi:10.1016/S0376-7388(01)00356-8.
- 50 R.F. Fedors, A method for estimating both the solubility parameters and molar volumes of liquids, *Polym. Eng. Sci.* 14 (1974) 147–154. doi:10.1002/pen.760140211.
- 51 D.W.van Krevelen, *Cohesive Properties and Solubility, Properties of Polymers*, 4th Edn., Elsevier, Amsterdam. (2008) 189–227, NL.
- 52 G. Schock, A. Miquel, Mass transfer and pressure loss in spiral wound modules, *Desalination.* 64 (1987) 339–352. doi:10.1016/0011-9164(87)90107-X.

- 53 A. Bouchoux, H. Roux-de Balmann, F. Lutin, Nanofiltration of glucose and sodium lactate solutions : variations of retention between single- and mixed-solute solutions, *J. Membrane Sci.* 258 (2005) 123–132. doi:10.1016/j.memsci.2005.03.002.
- 54 H. Schlichting, *Boundary layer theory*, McGraw-Hill Book Co. Inc., New York, (1960), USA.
- 55 C.P. Koutsou, S.G. Yiantsios, A.J. Karabelas, Direct numerical simulation of flow in spacer-filled channels: Effect of spacer geometrical characteristics, *J. Membrane Sci.* 291 (2007) 53–69. doi:10.1016/j.memsci.2006.12.032.
- 56 B.E. Eaton, Analysis of laminar vortex shedding behind a circular cylinder by computer-aided flow visualization, *J. Fluid Mech.* 180 (1987) 117. doi:10.1017/S0022112087001757.
- 57 G.E. Karniadakis, B.B. Mikic, A.T. Patera, Minimum-dissipation transport enhancement by flow destabilization: Reynolds' analogy revisited, *J. Fluid Mech.* 192 (1988) 365. doi:10.1017/S0022112088001909.
- 58 A.J. Karabelas, M. Kostoglou, C.P. Koutsou, Modeling of spiral wound membrane desalination modules and plants – review and research priorities, *Desalination.* 356 (2015) 165–186. doi:10.1016/j.desal.2014.10.002.
- 59 J. Luo, Y. Wan, Effects of pH and salt on nanofiltration—a critical review, *J. Membrane Sci.* 438 (2013) 18–28. doi:10.1016/j.memsci.2013.03.029.
- 60 E. Idil Mouhoumed, Études des propriétés de charge et de transport de membranes de nanofiltration, PhD report, Thèse de l'université de Rennes 1, France, 2016.
- 61 Landolt-Börnstein/Roth-Scheel, *Physikalisch-Chemische Tabellen*, Fünfte umgearbeitete und vermehrte Auflage, Berlin, Verlag von Julius Springer, 1927
- 62 E.S. Tarleton, J.P. Robinson, M. Salman, Solvent-induced swelling of membranes — Measurements and influence in nanofiltration, *J. Membrane Sci.* 280 (2006) 442–451. doi:10.1016/j.memsci.2006.01.050.
- 63 M. Amirilargani, M. Sadrzadeh, E.J.R. Sudhölter, L.C.P.M. de Smet, Surface modification methods of organic solvent nanofiltration membranes, *Chem. Eng. J.* 289 (2016) 562–582. doi:10.1016/j.cej.2015.12.062.
- 64 S. Postel, G. Spalding, M. Chirnside, M. Wessling, On negative retentions in organic solvent nanofiltration, *J. Membrane Sci.* 447 (2013) 57–65. doi:10.1016/j.memsci.2013.06.009.

Figures captions

Fig. 1: Equivalent molar volumes of BGS calculated from density of pure solvents and from eq. 18.

Fig. 2: Osmotic pressure at 20 C calculated according to van't Hoff equation (■) and taking into account virial expansion reduced at its first terms (eq. 17) in the range of the present study with $B' = V_m$ (▲) and $B' = V_{m,BGS}$ (Δ), (Table 3, Table 4).

Fig. 3: Experimental flux (J_p) of water/alcohol mixtures during NF in standard conditions - (a) J_p water/isopropanol vs TMP – (b) slope of (J_p vs TMP) vs alcohol content– © slope of (J_p vs TMP) vs viscosity of the water/alcohol mixtures.

Fig. 4: Experimental Rejections (R_{exp}) of alcohols during NF of water/alcohol mixtures in standard conditions

Fig. 5: Attempt of correlation between experimental rejections and Hansen-Hildebrand parameters of alcohol and membrane.

Fig. 6: Modelling of alcohol rejection in water/alcohol mixtures according to the approach coupling solution diffusion and film equations (SD-F).

Fig. 7: Modelling of alcohol rejection in water/alcohol mixtures according to the approach coupling Spiegler & Kedem and film equations (SK-F).

Fig. 8: C_m/C_b polarisation coefficient during NF of water/alcohol mixtures as calculated according to combination of Spiegler & Kedem and film (SK-F).

Fig. 9: Attempt of correlation between physico-chemical parameters of the water/alcohol mixtures (Table 3) and the apparent pore radius (see also Fig. S6-1 in supplementary 6).

Fig. 10: Membrane resistance in water and water/alcohol ($R_{m,BGS}$) calculated from $\Delta\pi_{obs}$, according to assumption on B' in virial expansion (see Table 4): ■: van't Hoff, ▲: $B' = V_m$, Δ: $B' = V_{m,BGS}$

Fig. 11: the $\Delta x/A_k$ ratio variation determined from eq. 24, using the $R_{m,BGS}$ value for $B' = V_m$ (Fig. 10) and membrane pore radius of Table 8 (simultaneously determined value)

Table captions

Table 1: Parameters required for calculations and deduced by the different models: Solution Diffusion + Film (SD-F), Spiegler & Kedem + Film (SK-F), Steric Hindrance pore (SHP)

Table 2: Properties of pure solvents (Stokes radius in water ($r_{s,Stokes}$), viscosity η , density ρ , Hildebrand solubility parameter δ , molar volume V_m at 20°C.

Table 3 : Properties of water/alcohol mixtures (BGS) at 20°C: viscosity η_{BGS} , diffusion coefficient of alcohol in the polarization layer taking into account slight polarisation $D_{alcohol}$, density, ρ_{BGS} (eq. 20), Hansen-Hildebrand solubility parameter (eq. 21), δ_{BGS} and equivalent molar volume $V_{m,BGS}$ of the solvent mixture (eq. 18).

Table 4: selected B' values ($10^{-5} \text{ m}^3 \cdot \text{mol}^{-1}$) according to assumptions

Table 5: Quality of alcohols

Table 6: Value of mass transfer coefficients obtained by SD-F model

Table 7: Value of mass transfer coefficients obtained by SK-F model

Table 8: Solute and pore radii (in nm) according to different assumptions

Table 9: Estimation of average apparent pore radius for a given viscosity regardless of the alcohol

Table 10: R_m and average $R_{m,BGS}$ for the different water/alcohol mixtures

Journal Pre-proof

Highlights

- NF270 exhibits a selectivity between water and alcohol increasing with alcohol size
- Alcohols' rejections cannot be modelled by coupling Solution Diffusion and film models
- Alcohols' rejections are nicely modelled by coupling Spiegler & Kedem and film equations
- Viscosity & osmotic pressure have an impact on flux contrary to concentration polarisation
- Pore size & membrane thickness increase can compensate leading to a constant resistance

Journal Pre-proof

Journal Pre-proof

Work was equally shared between the authors

Journal Pre-proof